
Functional Distribution Networks (FDN)

Omer Haq^{*1}

Abstract

Modern probabilistic regressors often remain overconfident under distribution shift. Functional Distribution Networks (FDN) place input-conditioned distributions over network weights, producing predictive mixtures whose dispersion adapts to the input; we train them with a Monte Carlo β -ELBO objective. We pair FDN with an evaluation protocol that separates interpolation from extrapolation and emphasizes simple OOD sanity checks. On controlled 1D tasks and small/medium UCI-style regression benchmarks, FDN remains competitive in accuracy with strong Bayesian, ensemble, dropout, and hypernetwork baselines, while providing strongly input-dependent, shift-aware uncertainty and competitive calibration under matched parameter and update budgets.

1. Introduction

Modern neural predictors are often deployed under dataset shift, where test inputs depart from the training distribution. In such regimes, deterministic networks and common stochastic heuristics frequently become *overconfident*, assigning high probability to incorrect predictions far from the training support and undermining reliable decision making. Bayesian Neural Networks (BNNs), MLPs with dropout, Deep Ensembles, and Hypernetworks are strong practical baselines, yet they can still under-react under shift or require substantial ensembling or sampling to achieve robust uncertainty behavior (Quiñero-Candela et al., 2009; Ovadia et al., 2019; Guo et al., 2017; MacKay, 1992; Neal, 1996; Graves, 2011; Blundell et al., 2015; Gal & Ghahramani, 2016; Lakshminarayanan et al., 2017; Ha et al., 2017).

This motivates architectures that are explicitly *uncertainty-aware* and *calibrated*, producing sharp predictions in-distribution (ID) while widening appropriately under dis-

tribution shift. We pursue this goal with *Functional Distribution Networks (FDN)*, which place input-conditioned distributions over network weights, allowing predictive uncertainty to adapt locally in input space. FDN amortizes an input-conditional posterior $q_\phi(\theta | x)$ via small hypernetworks and is trained using a Monte Carlo likelihood and a β -ELBO objective.

Empirically, under matched parameter and inference budgets, FDN is ID-competitive and exhibits strong calibration under shift. On controlled 1D regression tasks, predictive variance closely tracks error growth in- and out-of-distribution, while on more challenging oscillatory shifts FDN preserves rank calibration and increases uncertainty OOD, albeit with some under-scaling. We further evaluate FDN on standard UCI-style regression benchmarks—Airfoil Self-Noise, Combined Cycle Power Plant, and Energy Efficiency (Brooks et al., 1989; Tüfekci & Kaya, 2014; Tsanas & Xifara, 2012)—where it typically widens uncertainty under feature-based shifts while maintaining competitive accuracy and calibration relative to strong Bayesian, ensemble, and hypernetwork baselines.

Overview. Rather than treating weights as fixed (or globally random), FDN places an input-conditioned distribution over weights:

$$\theta | x \sim p(\theta | x), \quad y | x, \theta \sim p(y | x, \theta).$$

For tractability we fix an input-agnostic prior $p(\theta | x) = p_0(\theta) = \mathcal{N}(0, \sigma_0^2 I)$, so all input dependence is carried by an amortized posterior $q_\phi(\theta | x)$ implemented via small Hypernetworks. Many standard uncertainty-aware architectures can be cast in this template via different choices of $q_\phi(\theta | x)$; we detail these instantiations in Appendix A. Sampling $\theta \sim q_\phi(\theta | x)$ yields locally adaptive functions, and as x moves off the training support the induced weight distribution can broaden, producing wider and more appropriately uncertain predictive densities.

Training and evaluation. We train with a Monte Carlo β -ELBO over $q_\phi(\theta | x)$ and also report an IWAE variant; explicit expressions for the layer-wise KL and its LP-FDN factorization are given in the Appendix B. Our evaluation protocol splits test points into interpolation (ID) and extrapolation (OOD) regions and summarizes shift via deltas

¹Independent Researcher, Baltimore, MD, USA. Correspondence to: Omer Haq <haqomer1@gmail.com>.

$\Delta(\cdot) = \mathbb{E}_{\text{OOD}}[\cdot] - \mathbb{E}_{\text{ID}}[\cdot]$, focusing on ΔMSE , ΔVar , and ΔCRPS together with MSE–variance fits and risk–coverage curves.

Contributions. (i) **Model.** We introduce Functional Distribution Networks (FDN), a simple module that amortizes input-conditioned weight distributions via small Hypernetworks, in two variants: IC-FDNet (conditioning on x) and LP-FDNet (conditioning layer-wise on previous activations). (ii) **Protocol.** We propose a small-suite extrapolation protocol that targets $\Delta\text{Var} > 0$ under shift and complements it with calibration diagnostics (MSE–variance slope, rank correlation, and risk–coverage). (iii) **Empirical study.** Under matched parameter, update, and predictive-sample budgets, we benchmark FDN against strong Bayesian, ensemble, dropout, and hypernetwork baselines on controlled 1D function families and UCI-style regression tasks, showing that FDN remains ID-competitive while providing practically useful, shift-aware uncertainty.

Scope. We focus on low-dimensional regression with homoscedastic scalar Gaussian heads and relatively shallow backbones in order to isolate ID vs. OOD behavior under tightly matched budgets. All code, configurations, and scripts to reproduce the experiments will be released upon acceptance.

2. Related Work

Uncertainty in neural regression. BNN place distributions over weights and infer posteriors via variational approximations or MCMC (MacKay, 1992; Neal, 1996; Graves, 2011; Blundell et al., 2015). Deep Ensembles average predictions from independently trained networks and are a strong practical baseline (Lakshminarayanan et al., 2017; Maddox et al., 2019). MLP (with dropout) interprets dropout at test time as approximate Bayesian inference (Gal & Ghahramani, 2016). Heteroscedastic regression learns input-dependent output variance but retains deterministic weights (Nix & Weigend, 1994; Kendall & Gal, 2017).

Hypernetworks and conditional weight generation. Hypernetworks generate the weights of a primary network using an auxiliary network (Ha et al., 2017); related work explores dynamic, input-conditioned filters and conditional computation (De Brabandere et al., 2016; Brock et al., 2018). Bayesian/uncertainty-aware Hypernetworks place distributions over generated weights and train them variationally (Krueger et al., 2017). Our FDN differs by explicitly conditioning the weight distributions on the current input (or intermediate activations) in order to modulate epistemic uncertainty itself, not only deterministic weights. This input-aware weight stochasticity is what enables FDN to widen uncertainty under distributional shift while maintaining competitive ID accuracy under matched budgets.

Calibration and OOD behavior. Proper scoring rules such as the continuous ranked probability score (CRPS) are strictly proper and reward calibrated predictive distributions (Gneiting & Raftery, 2007). Empirical studies highlight overconfidence under dataset shift and introduce OOD benchmarks (Ovadia et al., 2019). Our evaluation therefore separates interpolation from extrapolation and uses the monotonic relationship between per-sample squared error (MSE) and predicted variance as a simple diagnostic calibration check.

Positioning. Compared to BNNs, FDN sidesteps global posteriors by amortizing *local* weight distributions $q_\phi(\theta | x)$. Compared to Deep Ensembles, FDN uses shared parameters and stochastic generation instead of replicating full models. Compared to Hypernetworks, FDN explicitly models *uncertainty over* generated weights and regularizes it with a KL prior, enabling principled OOD expansion.

3. Method

For convenience, a summary of the main symbols and dimensions used throughout the paper is provided in Table 1 in Appendix C.

3.1. Preliminaries

We model $y \in \mathbb{R}^{d_y}$ with a neural network $f_\theta : \mathbb{R}^{d_x} \rightarrow \mathbb{R}^{d_y}$ whose final layer parametrizes a Gaussian predictive head $(\mu_\theta(x), \Sigma_\theta(x))$, yielding

$$p(y | x, \theta) = \mathcal{N}(y; \mu_\theta(x), \Sigma_\theta(x)).$$

In the main experiments we use a homoscedastic Gaussian likelihood $p(y | x, \theta) = \mathcal{N}(y; \mu_\theta(x), \sigma^2)$ with fixed variance σ^2 , shared across all models. This removes aleatoric uncertainty and isolates epistemic uncertainty arising from stochastic weights. Under this likelihood, the β -ELBO reduces (up to constants) to a weighted squared-error term plus a KL penalty, yielding a $MSE + \beta KL$ objective. We use the same Gaussian head for all baselines to ensure a fair comparison.

More general likelihoods are discussed in Appendix D.

3.2. FDN: Input-Conditioned Weight Distributions

We drop explicit context and condition only on signals from the network itself. For each layer ℓ , FDN places a diagonal-Gaussian over its weights whose parameters are produced by a small Hypernetwork $A_\ell(\cdot)$. We choose the conditioning signal

$$s_\ell^{(k)} \in \begin{cases} x, & \text{IC-FDN} \\ a_{\ell-1}^{(k)}, & \text{LP-FDN (with } a_0^{(k)} = x), \end{cases}$$

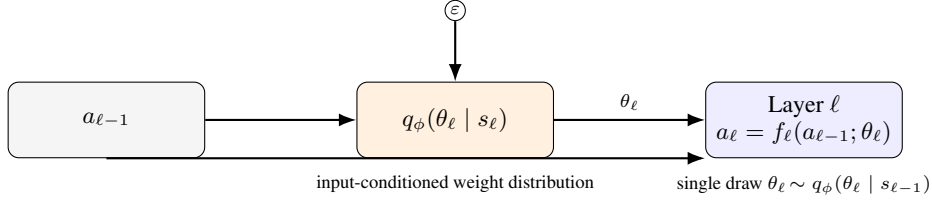


Figure 1. Single-layer view of FDN. For layer ℓ , the previous activation $a_{\ell-1}$ (with $a_0 = x$ for the first layer) is fed to both the hypernetwork and the main layer. For IC-FDN $s_{\ell} = x$ while for LP-FDN $s_{\ell} = a_{\ell-1}$. The hypernetwork takes s_{ℓ} and a random draw ϵ to generate weights/biases (Gaussian Head with reparameterization technique) $\theta_{\ell} = (W_{\ell}, b_{\ell})$, which are then used by the main layer $a_{\ell} = f_{\ell}(a_{\ell-1}; \theta_{\ell})$.

and set

$$(\mu_{W,\ell}, \rho_{W,\ell}, \mu_{b,\ell}, \rho_{b,\ell}) = A_{\ell}(s_{\ell}^{(k)}),$$

where $\sigma_{\cdot,\ell} = \epsilon + \text{softplus}(\rho_{\cdot,\ell})$, with a small variance floor $\epsilon = 10^{-3}$ for numerical stability. Sampling then proceeds via the standard Gaussian reparameterization trick. The conditioning signal is chosen as $s_{\ell} = x$ for IC-FDN and $s_{\ell} = a_{\ell-1}^{(k)}$ for LP-FDN, where in both cases the layer output is $a_{\ell}^{(k)} = f_{\ell}(a_{\ell-1}^{(k)}; W_{\ell}^{(k)}, b_{\ell}^{(k)})$ (sequential across layers). Figure 1 illustrates a single FDN layer: a small hypernetwork maps s_{ℓ} to the parameters of a Gaussian distribution over weights and biases; a sample $\theta_{\ell} = (W_{\ell}, b_{\ell})$ from this distribution is then used to compute $a_{\ell} = f_{\ell}(a_{\ell-1}; \theta_{\ell})$.

Variational family (compact). FDN uses a layer-wise diagonal-Gaussian over weights, conditioned on $s_{\ell} \in \{x, a_{\ell-1}^{(k)}\}$:

$$q_{\phi}(\theta | x) = \prod_{\ell=1}^L \mathcal{N}((W_{\ell}, b_{\ell}); (\mu_{W,\ell}, \mu_{b,\ell}), \text{diag}(\sigma_{W,\ell}^2, \sigma_{b,\ell}^2)).$$

In compact form (concatenating all layers),

$$q_{\phi}(\theta | x) = \mathcal{N}(\theta; \mu_{\phi}(x), \text{diag} \sigma_{\phi}^2(x)),$$

and the predictive density is the Monte Carlo mixture

$$p(y | x) \approx \frac{1}{K} \sum_{k=1}^K p(y | x, \theta^{(k)}), \quad \theta^{(k)} \sim q_{\phi}(\theta | x).$$

Prior and regularization. We regularize $q_{\phi}(\theta | x)$ toward a simple reference $p_0(\theta) = \prod_{\ell} \mathcal{N}(0, \sigma_0^2 I)$ via a β -weighted KL term (we use $\sigma_0 = 1$ in all experiments). For diagonal Gaussians,

$$KL(\mathcal{N}(\mu, \text{diag} \sigma^2) \| \mathcal{N}(0, \sigma_0^2 I)) = \frac{1}{2} \sum_j KL_j,$$

where $KL_j = (\sigma_j^2 + \mu_j^2)/\sigma_0^2 - 1 - \log(\sigma_j^2/\sigma_0^2)$. We sum this over all layers and parameters (both W_{ℓ} and b_{ℓ}).

Algorithm 1 (Appendix E) summarizes training (β -ELBO with re-parameterized gradients) and inference (Monte-Carlo mixtures over weight draws) for both IC-FDN and LP-FDN.

IC-FDN vs. LP-FDN. We study two conditioning schemes. *IC-FDN* (Input-Conditioned) uses the raw input x at every layer, $s_{\ell}(x) = x$, so all layers see the same features when sampling weights. *LP-FDN* (Layer-Progressive) instead uses hidden activations, with $s_0(x) = x$ and $s_{\ell}(x) = a_{\ell-1}(x)$ for $\ell \geq 1$, yielding a depth-aware conditioning scheme. Empirically, the two variants achieve similar in-distribution accuracy across our benchmarks, while LP-FDN often produces somewhat larger increases in predictive variance under distribution shift (larger ΔVar) at comparable MSE.

4. Experiments

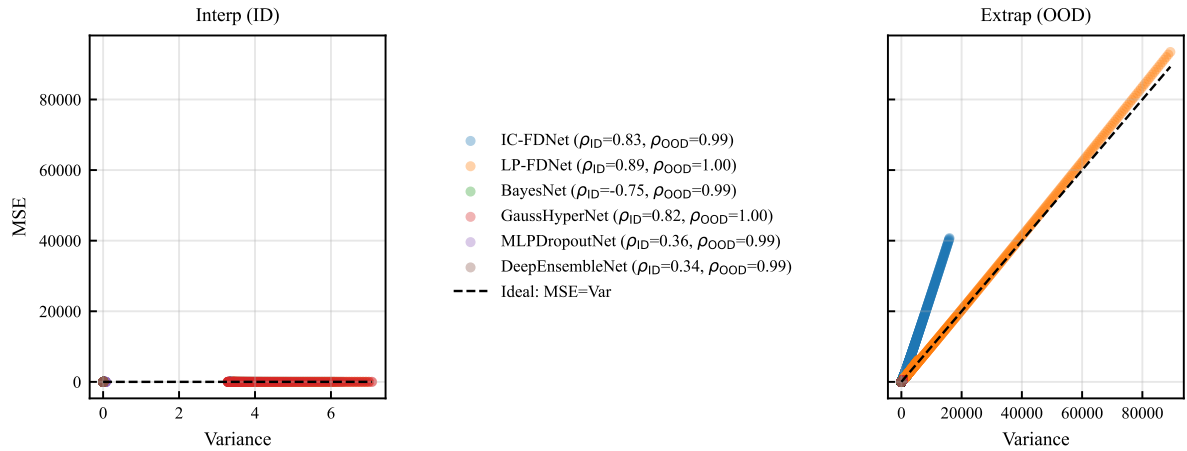
Tasks and splits. We evaluate FDN on (i) controlled 1D regression tasks where the ground-truth function is known and interpolation vs. extrapolation is precisely defined in input space, and (ii) standard UCI-style regression benchmarks with feature-based ID/OOD splits. In both settings we report metrics separately on the interpolation (ID) region, the extrapolation (OOD) region, and the aggregated test set, and we summarize distribution shift by deltas $\Delta(\cdot) = \mathbb{E}_{\text{OOD}}[\cdot] - \mathbb{E}_{\text{ID}}[\cdot]$.

4.1. Toy function families and ID/OOD protocol

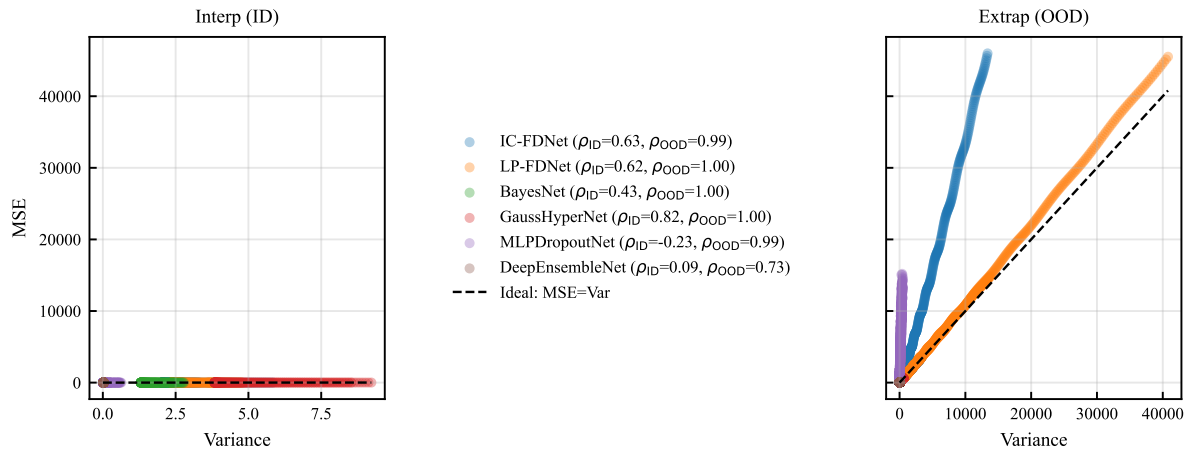
We first benchmark on 1D toy regression tasks, where the ground-truth function $f: \mathbb{R} \rightarrow \mathbb{R}$ is known. For each run we select one of three families:

- **Step:** $f(x) = H(x) = \mathbf{1}\{x \geq x_0\}$, with a discontinuity at $x_0 = 0$.
- **Sine:** $f(x) = A \sin(\omega x)$, with amplitude A and frequency ω .
- **Quadratic:** $f(x) = ax^2 + b$, with (a, b) fixed across runs.

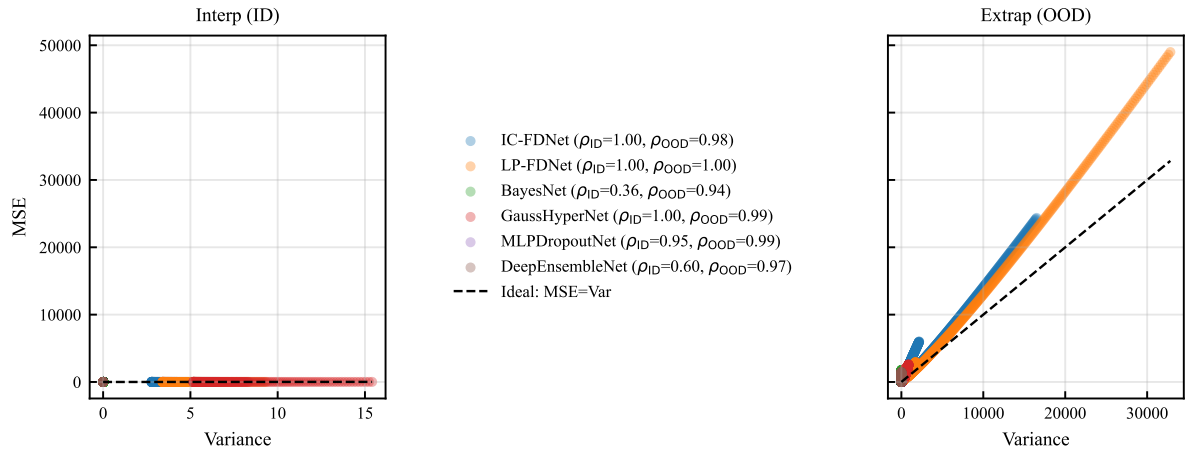
Unless otherwise stated we use the specific instantiations shown in Figure 2 (step $H(x)$, sine $1.54 \sin(2.39x)$, and quadratic $0.43x^2 - 0.41$) to match all reported plots. We define a symmetric interpolation region $R_{\text{interp}} = [-\ell, \ell]$



(a) Step: $H(x)$

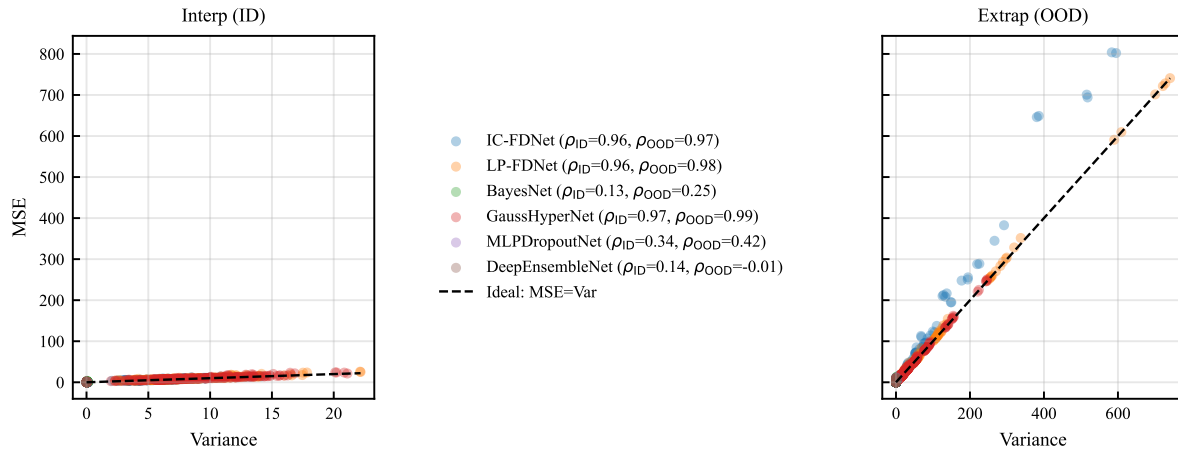


(b) Sine: $1.54 \sin(2.39x)$

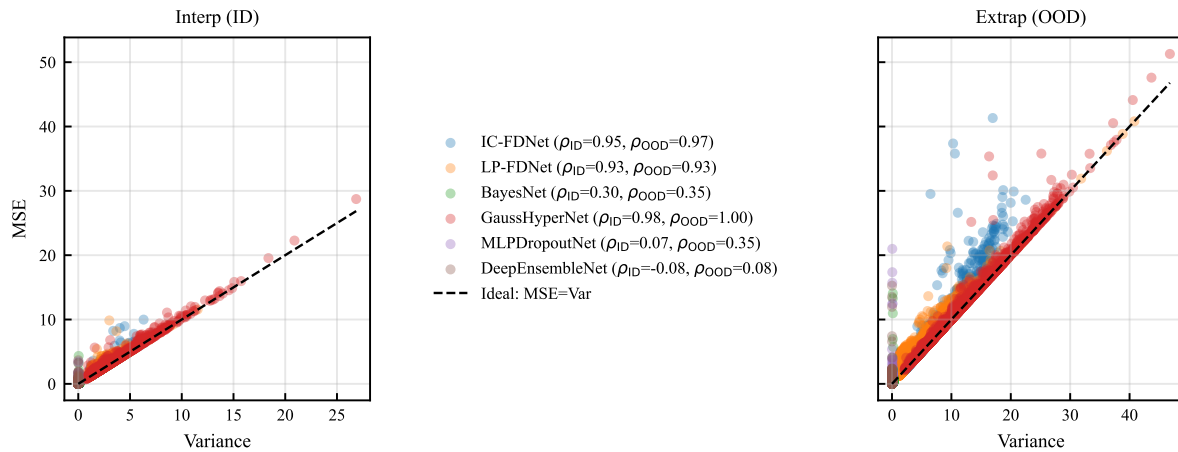


(c) Quadratic: $0.43x^2 - 0.41$

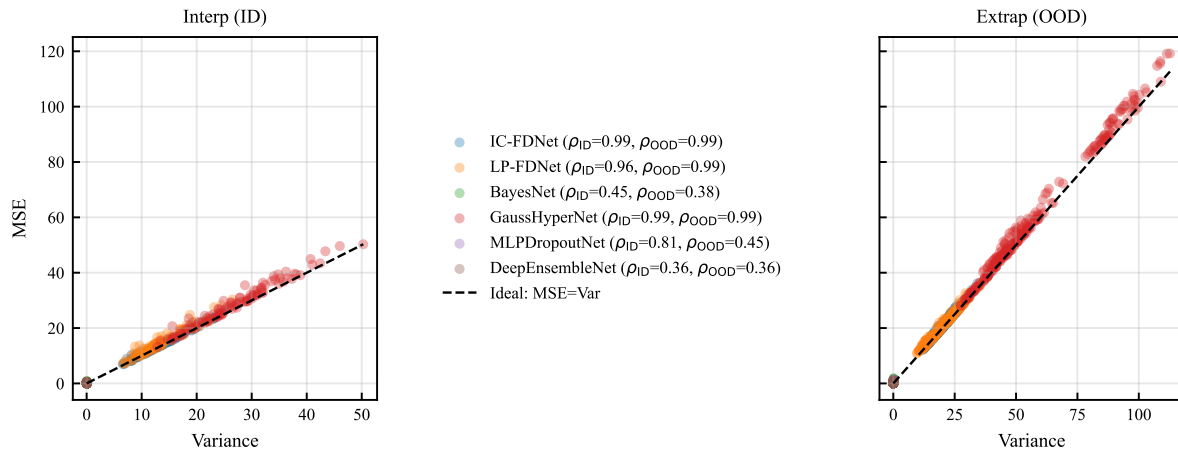
Figure 2. MSE vs. predicted variance on three 1D regression tasks (rows: step, sine, quadratic). Left/right panels in each row show interpolation (ID) and extrapolation (OOD) test points with shared axes; the dashed line marks the ideal $MSE = Var$. Legends report per-model Spearman's ρ in each region.



(a) Airfoil Self-Noise

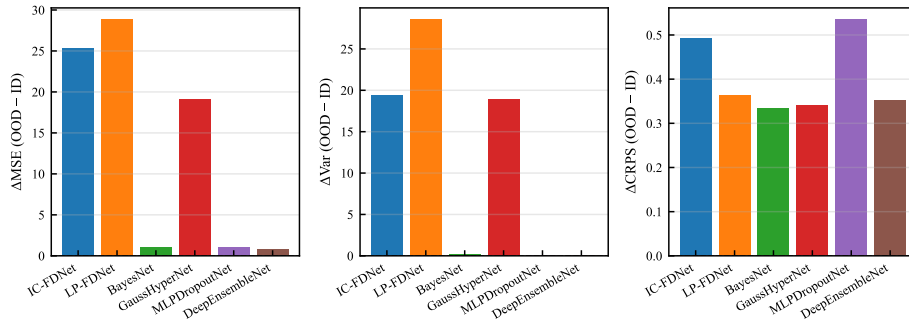


(b) CCPP Power Plant

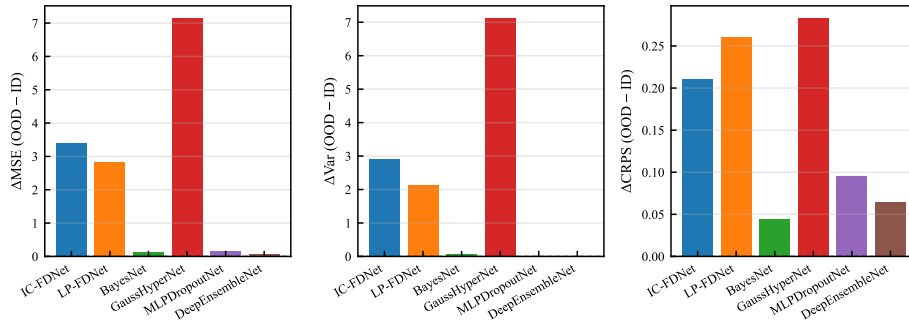


(c) Energy Efficiency Heating

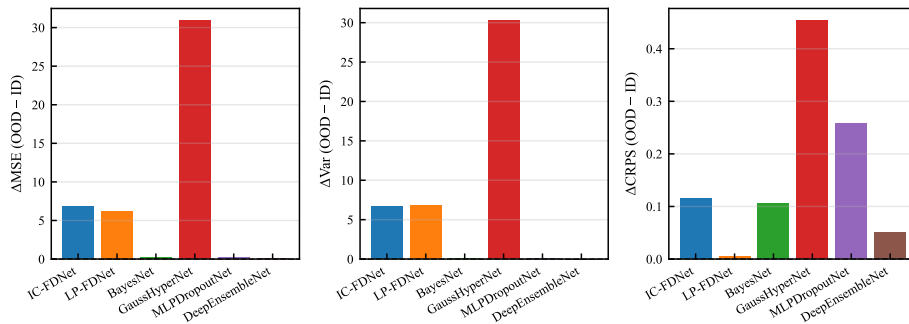
Figure 3. MSE vs. predicted variance on three real regression datasets: Airfoil Self-Noise, CCPP Power Plant, and Energy Efficiency (heating). For each dataset, left/right panels show ID and OOD test points with shared axes, and the dashed line marks $MSE = Var$. Legends report per-model Spearman's ρ .



(a) Airfoil Self-Noise



(b) CCPP Power Plant



(c) Energy Efficiency Heating

Figure 4. ID→OOD deltas on the real regression datasets. Bars show ΔMSE , ΔVar , and ΔCRPS for Airfoil, CCPP, and Energy. Well-behaved models exhibit large positive ΔVar together with moderate ΔMSE and ΔCRPS , indicating that uncertainty widens under shift while accuracy and calibration degrade gracefully.

and an extrapolation region $R_{\text{extrap}} = \mathbb{R} \setminus R_{\text{interp}}$. Training and validation inputs are sampled uniformly from R_{interp} ; test inputs cover both R_{interp} and R_{extrap} on a dense grid. We report all metrics separately on the ID split (test points in R_{interp}), the OOD split (test points outside R_{interp}), and on the full test set. This protocol ensures that “OOD” strictly corresponds to extrapolation in input space.

4.2. Real regression datasets and ID/OOD splits

To test FDNs beyond 1D toy functions we use three standard UCI regression datasets: Airfoil Self-Noise, Combined Cycle Power Plant (CCPP), and Energy Efficiency (heating load as the primary target). For each dataset we follow a consistent preprocessing and ID/OOD protocol: we choose a single “ID feature” z with a natural interpretation (e.g., frequency for Airfoil, ambient temperature for CCPP, relative compactness for Energy), define the interpolation band as the 20th–80th percentiles of this feature and treat the extremes as extrapolation, split train/validation/test by quantiles of z , and standardize all inputs and targets using training statistics. We fix a single train/validation/test split shared across all methods and seeds. Exact dataset sizes are summarized in Table 3 (Appendix F).

4.3. Complexity, capacity, and fairness

Baselines. We evaluate four stochastic baselines: MLP with dropout (**MLPDropoutNet**), Deep Ensemble of MLP (**DeepEnsemblesNet**), Variational BNN (**BayesNet**), and Gaussian Hypernetwork (**GaussianHyperNet**). Because our study centers on calibrated *predictive distributions* (CRPS, MSE–Var slope/intercept, AURC), we omit the **Deterministic MLP** and the (input-conditioned) **Hypernetwork** from the main uncertainty analysis; their ID/OOD MSE is comparable to Ensembles/Dropout. Training details (optimizer, batch size, learning rate, prior scale σ_0 , variance floor σ_{\min}) appear in Table 2 (Appendix F).

Link-budget. We consider networks with a single hidden layer and fix the parameter budget to $P \approx 1000$ ($\pm 5\%$) for all models, counting *all* trainable parameters, including any Hypernetwork components; counts appear in Table 4 (Appendix F). To equalize the *update* budget, ensembles with M members use *epoch-split* training (epochs divided by M). For non-ensemble networks we use one Monte Carlo draw per update ($K = 1$), keeping per-step cost comparable and the total number of parameter updates matched across models.

Note: To hit the P target, MLPDropoutNet uses widened hidden layers, increasing capacity/expressive power and potentially improving ID MSE independent of uncertainty quality; hence our emphasis on calibration-centric metrics.

Computational complexity and scalability. For all models, the per-epoch training cost scales linearly in the number of examples N and quadratically in the layer widths, $O(N \sum_{\ell} d_{\ell-1} d_{\ell})$. Both IC-FDN and LP-FDN inherit this scaling from the base MLP: the per-layer Hypernetworks add only a small constant-factor overhead because their hidden width h_{hyp} and the Monte Carlo count K are fixed (parameter count remains $O(d_{\ell-1} d_{\ell})$ per layer), matching the baselines. A full discussion of parameter-count and architectural trade-offs for larger models are given in Appendix G.

4.4. Metrics and calibration diagnostics

We assess models with standard metrics for accuracy, uncertainty, and calibration: mean squared error (MSE), predictive variance, continuous ranked probability score (CRPS), risk–coverage curves (area under the risk–coverage curve, AURC), and ID→OOD deltas (ΔMSE , ΔVar , ΔCRPS). For calibration we use both rank- and scale-based diagnostics: (i) Spearman correlation $\rho(\text{Var}, \text{MSE})$ between per-point variance and squared error, and (ii) a linear fit $\text{MSE} \approx a + b \text{Var}$, with the ideal calibration corresponding to $a \approx 0$ and $b \approx 1$. We visualize these diagnostics via MSE–Var scatter plots in the ID and OOD regions for toy tasks (Figure 2) and real datasets (Figure 3), together with grouped bar charts of ID→OOD deltas on the real tasks (Figure 4). Precise definitions and Monte Carlo estimators for all metrics are collected in Appendix H.

Representative seed selection. To avoid cherry-picking, all qualitative plots are based on a *representative* seed selected by a fixed aggregation rule. For each dataset and configuration, we run all models over multiple random seeds (20 for toy tasks, 100 for Airfoil, and 3 for the remaining UCI datasets) and compute per-seed summary metrics (e.g., ID/OOD MSE, variance, ΔCRPS , AURC). For IC-FDNet (or LP-FDNet), we take the coordinate-wise median of these metrics and select the seed whose metric vector is closest (Euclidean distance) to this median. All qualitative plots use this representative seed under the same rule across datasets, ensuring the shown behavior is typical rather than hand-picked. For Airfoil, Figure 5 (Appendix F) confirms that the selected seed lies close to the overall across-seed trend.

4.5. Results

Toy tasks. Across the three toy tasks (Tables 5–7; Figure 2), FDN’s core strength is scale calibration under smooth shifts. On the step and quadratic tasks, IC-/LP-FDNet achieve MSE–Var slopes closer to the ideal $b \approx 1$ with strong rank agreement (Spearman ρ close to 1) and large positive ΔVar , so predictive variance increases in lock-step with difficulty. This comes at the cost of higher AURC and ΔCRPS than the sharpest baselines on the step task,

while on the quadratic task their AURC and Δ CRPS are broadly comparable. In contrast, several classical baselines that fit ID sharply (e.g., Deep Ensembles, BayesNet) exhibit much steeper MSE–Var fits ($b \gg 1$) and smaller increases in variance (Δ Var), indicating sharper but less conservative uncertainty even when they rank hard points reasonably well.

On the highly oscillatory sine shift, all methods degrade, but the trade-offs differ. FDN preserves excellent ranking (Spearman ρ near 1) and raises variance substantially OOD (large Δ Var), yet its error grows faster than its variance (large b , large Δ MSE), yielding worse AURC. Deep ensembles show smaller Δ MSE and hence better AURC, but their ranking can be weaker. Overall, under matched capacity and update budgets, FDN’s main advantages are (i) calibrated scaling on smooth or piecewise-smooth shifts, where many baselines remain overconfident, and (ii) consistently high rank correlation across tasks, which makes FDN a strong triage signal even when absolute scale lags on rapidly oscillatory OOD. This highlights a clear avenue for improvement: stronger variance scaling on such shifts (e.g., temperature/flooring on σ_ϕ , richer priors, or layer-wise β schedules).

Real regression benchmarks. On the real regression tasks (Airfoil, CCPP, Energy), the same patterns largely persist (Figures 3 and 4; Tables 8–10). FDN achieves reasonable in-distribution MSE and typically exhibits large positive Δ Var, indicating that uncertainty widens under feature-based shift. This comes with somewhat larger Δ MSE and Δ CRPS than the sharpest baselines on Airfoil, but more moderate values on CCPP and Energy, so calibration degrades gradually rather than catastrophically. On Airfoil, for example, FDN’s ID scatter lies close to the ideal MSE=Var line and spreads out smoothly OOD, with strong Spearman correlation; on CCPP and Energy the predictive variances remain shift-aware and provide useful selective-risk behavior, even when the absolute scale is not always better than the strongest baselines. Taken together, the toy and UCI results suggest that input-conditioned weight stochasticity is a viable and modular route to OOD-aware regression: FDN behaves like a drop-in “uncertainty layer” that can be tuned via β and hypernetwork capacity to trade off in-distribution sharpness against OOD conservatism.

Additional qualitative diagnostics, including predictive means (Figure 6, 7), aggregated MSE–variance scatters (Figure 8, 9), and risk–coverage curves for all datasets (Figure 10, 11), are provided in (Appendix F).

5. Limitations

FDN’s input-conditioned *weight* stochasticity, like other stochastic layer designs, can overfit spurious cues if β is too

small or the prior is too loose, making careful KL scheduling and prior choice important. LP-FDN samples weights layer-by-layer, introducing additional latency relative to a deterministic forward pass; test-time sampling also incurs a compute–latency trade-off with the number of Monte Carlo samples K , though we keep K small in our experiments. Our study focuses on low-dimensional regression with tabular datasets and modest network backbones; extending FDN to high-dimensional inputs (e.g., images), deeper architectures, or structured outputs will likely require additional engineering, such as low-rank or adapter-style hypernetworks and tighter capacity control. On the calibration side, FDN can under-scale variance in highly oscillatory OOD regimes (e.g., the sine task), and the current design does not explicitly enforce frequency-aware or spectral robustness.

6. Conclusion

We introduced Functional Distribution Networks (FDN), which amortize input-conditioned distributions over weights to produce predictive densities that remain sharp in-distribution and expand under shift. Trained with a Monte Carlo objective and a β -weighted KL prior, FDN achieves strong rank calibration across tasks and near-ideal scale calibration on smooth and piecewise-smooth shifts, as measured by Spearman correlation, MSE–Var fit, Δ Var, Δ CRPS, and AURC. Under matched parameter, update, and sampling budgets, FDN is competitive with Bayesian, ensemble, dropout, and hypernetwork baselines on both 1D toy functions and UCI-style regression benchmarks, while providing uncertainty suitable for abstention and risk-aware inference.

Looking ahead, several directions are promising. On the modeling side, stronger variance-scaling mechanisms (e.g., temperature or layer-wise β scheduling, structured priors) and frequency-aware conditioning may reduce under-scaling on highly oscillatory OOD tasks. On the systems side, adapter-style deployments that apply FDN to a small subset of layers could inject uncertainty awareness into large-scale models with modest overhead. Finally, extending FDN to classification, sequence models, and structured prediction, or integrating it with other uncertainty-aware modules (e.g., Neural Processes or diffusion-style priors over weights), may enable a general toolkit for calibrated, shift-aware deep learning.

Impact Statement

This paper presents work whose goal is to advance the field of Machine Learning. There are many potential societal consequences of our work, none of which we feel must be specifically highlighted here.

References

- Alemi, A. A., Fischer, I., Dillon, J. V., and Murphy, K. Deep variational information bottleneck. In *International Conference on Learning Representations (ICLR)*, 2017.
- Blundell, C., Cornebise, J., Kavukcuoglu, K., and Wierstra, D. Weight uncertainty in neural networks. In *International Conference on Machine Learning (ICML)*, 2015.
- Brock, A., Lim, T., Ritchie, J. M., and Weston, N. Smash: One-shot model architecture search through hypernetworks. In *International Conference on Learning Representations (ICLR)*, 2018. URL <https://openreview.net/forum?id=rydeCEhs->.
- Brooks, T., Pope, D., and Marcolini, M. Airfoil self-noise. <https://doi.org/10.24432/C5VW2C>, 1989. UCI Machine Learning Repository.
- Burda, Y., Grosse, R., and Salakhutdinov, R. Importance weighted autoencoders. In *International Conference on Learning Representations (ICLR)*, 2016.
- De Brabandere, B., Jia, X., Tuytelaars, T., and Van Gool, L. Dynamic filter networks. In *Advances in Neural Information Processing Systems (NeurIPS)*, pp. 667–675, 2016.
- Dziugaite, G. K. and Roy, D. M. Computing nonvacuous generalization bounds for deep (stochastic) neural networks via pac-bayes. In *International Conference on Learning Representations (ICLR)*, 2017.
- Gal, Y. and Ghahramani, Z. Dropout as a bayesian approximation: Representing model uncertainty in deep learning. In *Proceedings of the 33rd International Conference on Machine Learning*, volume 48 of *Proceedings of Machine Learning Research*, pp. 1050–1059. PMLR, 2016.
- Gneiting, T. and Raftery, A. E. Strictly proper scoring rules, prediction, and estimation. *Journal of the Royal Statistical Society: Series B (Statistical Methodology)*, 69(2):243–268, 2007.
- Graves, A. Practical variational inference for neural networks. In *Advances in Neural Information Processing Systems (NeurIPS)*, 2011.
- Guo, C., Pleiss, G., Sun, Y., and Weinberger, K. Q. On calibration of modern neural networks. In *International Conference on Machine Learning (ICML)*, 2017.
- Ha, D., Dai, A., and Le, Q. V. Hypernetworks. In *International Conference on Learning Representations (ICLR)*, 2017. URL <https://openreview.net/forum?id=rkpACellx>.
- Higgins, I. et al. beta-VAE: Learning basic visual concepts with a constrained variational framework. In *International Conference on Learning Representations (ICLR)*, 2017.
- Houlsby, N., Giurgiu, A., Jastrzebski, S., Morrone, B., Laroussilhe, Q. D., Gesmundo, A., Attariyan, M., and Gelly, S. Parameter-efficient transfer learning for NLP. In *Proceedings of the 36th International Conference on Machine Learning*, pp. 2790–2799, 2019.
- Hu, E. J., Shen, Y., Wallis, P., Allen-Zhu, Z., Li, Y., Wang, S., Wang, L., and Chen, W. Lora: Low-rank adaptation of large language models. In *Proceedings of the 10th International Conference on Learning Representations*, 2022. URL <https://openreview.net/forum?id=nZeVKeeFYf9>.
- Kendall, A. and Gal, Y. What uncertainties do we need in bayesian deep learning for computer vision? In *Advances in Neural Information Processing Systems*, 2017.
- Krueger, D., Huang, C.-W., Islam, R., Turner, R., Lacoste, A., and Courville, A. Bayesian hypernetworks. *arXiv preprint arXiv:1710.04759*, 2017.
- Lakshminarayanan, B., Pritzel, A., and Blundell, C. Simple and scalable predictive uncertainty estimation using deep ensembles. In *Advances in Neural Information Processing Systems (NeurIPS)*, 2017.
- MacKay, D. J. C. A practical bayesian framework for back-propagation networks. *Neural Computation*, 4(3):448–472, 1992.
- Maddox, W., Garipov, T., Izmailov, P., Vetrov, D., and Wilson, A. G. A simple baseline for bayesian uncertainty in deep learning. In *Advances in Neural Information Processing Systems*, 2019.
- Neal, R. M. *Bayesian Learning for Neural Networks*, volume 118 of *Lecture Notes in Statistics*. Springer, 1996.
- Nix, D. A. and Weigend, A. S. Estimating the mean and variance of the target probability distribution. In *IEEE International Conference on Neural Networks*, 1994.
- Ovadia, Y., Fertig, E., Ren, J., Nado, Z., Sculley, D., Nowozin, S., Dillon, J., Lakshminarayanan, B., and Snoek, J. Can you trust your model’s uncertainty? evaluating predictive uncertainty under dataset shift. In *Advances in Neural Information Processing Systems (NeurIPS)*, 2019.
- Quiñonero-Candela, J., Sugiyama, M., Schwaighofer, A., and Lawrence, N. D. (eds.). *Dataset Shift in Machine Learning*. MIT Press, 2009.

Tsanas, A. and Xifara, A. Energy efficiency. <https://doi.org/10.24432/C51307>, 2012. UCI Machine Learning Repository.

Tüfekci, P. and Kaya, H. Combined cycle power plant. <https://doi.org/10.24432/C5002N>, 2014. UCI Machine Learning Repository.

A. Unified view via $q_\phi(\theta | x)$

All methods we consider can be written as

$$p(y | x) = \int p(y | x, \theta) q_\phi(\theta | x) d\theta \approx \frac{1}{K} \sum_{k=1}^K p(y | x, \theta^{(k)}), \quad \theta^{(k)} \sim q_\phi(\theta | x).$$

In this paper, architectural layers are specified by the choice of $q_\phi(\theta | x)$. Framing models through $q_\phi(\theta | x)$ enables apples-to-apples comparisons: (i) how they set the spread of plausible weights, (ii) whether that spread adapts to the input, and (iii) how much compute they expend to form the predictive mixture. FDN’s module-level approach directly targets this knob: it provides local, input-aware uncertainty where it is inserted (e.g., the head or later blocks), broadens off-support as inputs drift from the training domain, and leaves the surrounding backbone and training loop unchanged.

FDN (IC/LP) FDN makes q_ϕ **input-conditional and stochastic**. A common choice is diagonal-Gaussian, factorized by layer:

$$q_\phi(\theta | x) = \prod_{\ell} \mathcal{N}(\mu_\ell(x), \text{diag } \sigma_\ell^2(x)).$$

This **input-conditional** variant is *IC-FDN*. For **layer-propagated** conditioning (*LP-FDN*), the ℓ -th layer’s weight distribution depends *only* on the previous activation:

$$q_\phi(\theta_\ell | x) = \mathcal{N}(\mu_\ell(a_{\ell-1}), \text{diag } \sigma_\ell^2(a_{\ell-1})), \quad a_0 := x,$$

and sampling proceeds sequentially across layers along the same Monte Carlo sample path. This induces a first-order Markov structure in depth, allowing uncertainty to expand as signals propagate—later layers can broaden even when early layers remain sharp. We regularize with a per-layer KL:

$$\beta \sum_{\ell=1}^L KL(q_\phi(\theta_\ell | x) \| p_0(\theta_\ell)).$$

More generally, one could condition longer histories $a_{0:\ell-1}$; in this paper, we restrict to first-order (one-step) conditioning. Note, in the limit $\sigma_\ell \rightarrow 0$ for all ℓ , the model collapses to a deterministic layer-conditioned Hypernetwork.

Deterministic Hypernetwork. A deterministic Hypernetwork G_ϕ maps the input to weights, yielding a **degenerate** q :

$$q_\phi(\theta | x) = \delta(\theta - G_\phi(x)), \quad p(y | x) = p(y | x, G_\phi(x)).$$

Training typically uses NLL or MSE; weight decay on ϕ can be interpreted as a MAP prior on the Hypernetwork parameters. Because q_ϕ is a Dirac-Delta, there is no weight-space uncertainty: any predictive uncertainty must come from the observation model (e.g., a heteroscedastic head) or post-hoc calibration. Compared to stochastic variants, this adds no KL term and no MC averaging, but can increase per-example compute due to generating weights via G_ϕ .

Gaussian HyperNetwork A *Stochastic* Hypernetwork outputs a **global** posterior (or context-only):

$$q_\phi(\theta | x) \equiv q_\phi(\theta | h) = \prod_{\ell} \mathcal{N}(\mu_\ell(h), \text{diag } \sigma_\ell^2(h)),$$

i.e., independent of the query x (but dependent on a learnable latent task vector h). This is variational BNN with parameters produced by a Hypernetwork.

Bayesian Neural Network (Bayes-by-Backprop). A standard variational BNN uses an x -**independent** approximate posterior:

$$q_\phi(\theta | x) \equiv q_\phi(\theta) = \prod_{\ell} \mathcal{N}(\mu_\ell, \text{diag } \sigma_\ell^2),$$

and the same β -ELBO objective with closed-form diagonal-Gaussian KL. Because $q_\phi(\theta | x)$ is global, predictive uncertainty does not adapt to x except via the likelihood term, which can under-react off-support compared to input-conditional alternatives. On the other hand, the objective is simple and sampling cost is amortized across inputs, though matching ensemble-like diversity typically requires larger posterior variances or multiple posterior samples at test time.

MLP with Dropout. MLP with dropout induces a distribution over effective weights via random masks m :

$$q_\phi(\theta | x) \equiv q_\phi(\theta) \quad (\text{implicit via dropout masks, independent of } x),$$

and inference averages predictions over sampled masks (Gal & Ghahramani, 2016).

Deep Ensembles. An M -member ensemble of MLPs corresponds to a **finite mixture of deltas**:

$$q(\theta | x) \equiv \frac{1}{M} \sum_{m=1}^M \delta(\theta - \theta_m), \quad p(y | x) = \frac{1}{M} \sum_{m=1}^M p(y | x, \theta_m),$$

where each θ_m is trained independently from a different initialization (and typically a different data order/augmentation). There is no explicit KL regularizer; diversity arises implicitly from independent training trajectories. Inference cost scales linearly with M (one forward pass per member), and for fair comparisons we match total update or compute budgets by reducing epochs.

B. Training objective

FDN is amortized variational inference with the latent weights θ and input-conditional posterior $q_\phi(\theta | x)$ realized by small hypernetworks via the reparameterization $\theta^{(k)} = g_\phi(x, \varepsilon^{(k)})$ with $\varepsilon^{(k)} \sim \mathcal{N}(0, I)$. For a single (x, y) the ELBO is

$$\log p(y | x) \geq \underbrace{\mathbb{E}_{q_\phi(\theta|x)} [\log p(y | x, \theta)]}_{\text{data term}} - \underbrace{KL(q_\phi(\theta | x) \| p_0(\theta))}_{\text{regularizer}}, \quad (1)$$

with a simple prior $p_0(\theta) = \prod_\ell \mathcal{N}(0, \sigma_0^2 I)$.

(A) β -ELBO (mean of logs). We minimize the negative β -ELBO with K Monte Carlo draws:

$$\mathcal{L}_{\beta\text{-ELBO}} = -\frac{1}{K} \sum_{k=1}^K \log p(y | x, \theta^{(k)}) + \beta KL(q_\phi(\theta | x) \| p_0(\theta)), \quad \theta^{(k)} \sim q_\phi(\theta | x). \quad (2)$$

Here $\beta=1$ recovers standard VI; $\beta \neq 1$ implements capacity control / tempered VI (Higgins et al., 2017; Alemi et al., 2017; Dziugaite & Roy, 2017). We use simple warm-ups for β early in training.

(B) IWAE variant (log of means; tighter bound). As a reference, the importance-weighted bound is

$$\mathcal{L}_{\text{IWAE}} = -\log \left(\frac{1}{K} \sum_{k=1}^K \frac{p_0(\theta^{(k)}) p(y | x, \theta^{(k)})}{q_\phi(\theta^{(k)} | x)} \right), \quad \theta^{(k)} \sim q_\phi(\theta | x), \quad (3)$$

which implicitly accounts for the KL via the weights and typically needs no extra β (Burda et al., 2016). We report main results with (A) for simplicity and stability.

KL decomposition (IC vs. LP). For *IC-FDN*, layer posteriors condition directly on x , so the KL sums over layers and averages over the minibatch. For *LP-FDN*, layer ℓ conditions on a sampled hidden state $a_{\ell-1}^{(k)}(x)$; the KL is therefore averaged over this upstream randomness:

$$KL(q_{\phi,\ell}(\theta_\ell | a_{\ell-1}^{(k)}(x)) \| p_0) \quad \text{with} \quad \mathbb{E}_k[\cdot] \quad \text{across samples } k.$$

With diagonal Gaussians, each layer’s closed-form term is

$$KL(\mathcal{N}(\mu, \text{diag } \sigma^2) \| \mathcal{N}(0, \sigma_0^2 I)) = \frac{1}{2} \sum_j \left(\frac{\sigma_j^2 + \mu_j^2}{\sigma_0^2} - 1 - \log \frac{\sigma_j^2}{\sigma_0^2} \right),$$

and we implement the variance floor via $\sigma = \varepsilon + \text{softplus}(\rho)$ (no hard clamp).

Remark. Future work should investigate *layer-specific* β schedules to control where uncertainty is expressed across depth (e.g., larger β in early layers for stability, smaller β near the output to permit output-scale variance), with the aim of tightening scale calibration ($b \rightarrow 1$, $a \rightarrow 0$) and improving AURC/CRPS under oscillatory OOD.

C. Notation and symbols

Table 1. Key symbols, parameters, and dimensions used throughout the paper.

Symbol	Description	Dimension / Type
x	Input / covariate	\mathbb{R}^{d_x}
y	Target / response	\mathbb{R}^{d_y}
\mathcal{D}	Training dataset	$\{(x_i, y_i)\}_{i=1}^N$
N	Number of training examples	\mathbb{N}
T	Number of test examples	\mathbb{N}
d_x	Input dimension	scalar
d_y	Output dimension	scalar
D_y	Gaussian head output dim.	$\frac{d_y(d_y+3)}{2}$
f_θ	Base network (predictive head)	$f_\theta : \mathbb{R}^{d_x} \rightarrow \mathbb{R}^{D_y}$
θ	All base-network weights (all layers)	\mathbb{R}^P
ϕ	FDN / variational / hypernetwork params	parameter vector
$p(y x, \theta)$	Likelihood (Gaussian head)	$\mathcal{N}(y; \mu_\theta(x), \Sigma_\theta(x))$
$p_0(\theta)$	Weight prior	$\mathcal{N}(0, \sigma_0^2 I)$
$q_\phi(\theta x)$	Input-conditioned weight posterior	$\mathcal{N}(\mu_\phi(x), \text{diag } \sigma_\phi^2(x))$
β	KL weight in β -ELBO	scalar ≥ 0
$\mathcal{L}_{\beta\text{-ELBO}}$	Training loss (per-example)	scalar
L	Number of layers in base net	scalar
d_ℓ	Width of layer ℓ	scalar
s_ℓ	Conditioning signal for layer ℓ	$\mathbb{R}^{d_{s,\ell}}$
$d_{s,\ell}$	Dimension of s_ℓ	d_x (IC) or $d_{\ell-1}$ (LP)
A_ℓ	Per-layer hypernetwork	$A_\ell : \mathbb{R}^{d_{s,\ell}} \rightarrow \mathbb{R}^{P_\ell}$
P_ℓ	# Gaussian params for layer ℓ	$2(d_{\ell-1}d_\ell + d_\ell)$
P	Total # trainable parameters	$\sum_\ell P_\ell$ (plus head)
h_{hyp}	Hypernetwork hidden width	scalar
K	MC samples per input (train/test)	\mathbb{N}
M	Ensemble size (DeepEnsembleNet)	\mathbb{N}
σ_0	Prior std. for weights	scalar > 0
σ^2	Observation noise variance (homoscedastic)	scalar > 0
ε	Variance floor in $\sigma = \varepsilon + \text{softplus}(\rho)$	scalar > 0
$\hat{\mu}(x)$	Predictive mean	\mathbb{R}^{d_y}
$\widehat{\text{Var}}[Y x]$	Predictive variance estimator	scalar (for $d_y=1$)
MSE	Mean squared error	scalar
CRPS	Continuous ranked prob. score	scalar
NLL	Neg. log predictive density	scalar
ρ	Spearman rank correlation	scalar $\in [-1, 1]$
AURC	Area under risk-coverage curve	scalar
$\Delta(\cdot)$	ID \rightarrow OOD metric delta	$\mathbb{E}_{\text{OOD}}[\cdot] - \mathbb{E}_{\text{ID}}[\cdot]$

D. Heteroscedastic likelihood and variance decomposition

We briefly collect the forms of the Gaussian β -ELBO used in this work and the associated decomposition of predictive variance into epistemic and aleatoric components.

General Gaussian head. For a Gaussian predictive head with possibly heteroscedastic, full-covariance noise, the per-example β -ELBO for datum (x_i, y_i) is

$$\mathcal{L}_{\text{Gauss}}^{(i)} = \frac{1}{2K} \sum_{k=1}^K \left[\|y_i - \mu_{\theta_k}(x_i)\|_{(\Sigma_{\theta_k}(x_i))^{-1}}^2 + \log \det(2\pi \Sigma_{\theta_k}(x_i)) \right] + \beta KL(q_\phi(\theta | x_i) \| p_0(\theta)), \quad (4)$$

where $\|v\|_A^2 := v^\top A v$. In the *homoscedastic* case the covariance is constant across inputs, so a full Σ encodes a single, global correlation structure among output dimensions; if Σ is diagonal, the data term reduces to a (constant-)weighted

least-squares plus a constant log-determinant. In contrast, *heteroscedastic* models use an input-dependent $\Sigma_\theta(x)$, so the weights (and, for full $\Sigma_\theta(x)$, correlations) vary with x and with the sampled weights θ .

For $d_y = 1$ the covariance reduces to a scalar $\sigma_\theta^2(x)$. We say the noise is *homoscedastic in x* if $\sigma_\theta^2(x) \equiv \sigma_\theta^2$ (constant across inputs for a fixed θ), and *heteroscedastic in x* if $\sigma_\theta^2(x)$ varies with x . Orthogonally, because we draw stochastic weights $\theta^{(k)}$, one can distinguish dependence on the sampled weights: *homoscedastic in θ* means $\sigma_\theta^2(x)$ is effectively deterministic (identical across $\theta^{(k)}$ for a given x), while *heteroscedastic in θ* means $\sigma_{\theta^{(k)}}^2(x)$ changes with the sampled weights (as in FDN/BNN where the variance head depends on $\theta^{(k)}$).

In the **isotropic heteroscedastic** case, $\Sigma_{\theta^{(k)}}(x) = \sigma_{\theta^{(k)}}^2(x)I$, the Gaussian negative log-likelihood (NLL) contribution is

$$\frac{1}{2K} \sum_{k=1}^K \left[\left(\frac{y_i - \mu_{\theta^{(k)}}(x_i)}{\sigma_{\theta^{(k)}}(x_i)} \right)^2 + \log(2\pi \sigma_{\theta^{(k)}}^2(x_i)) \right], \quad (5)$$

i.e., a *per-input, per-sample weighted* MSE plus a variance penalty. If one instead assumes **isotropic homoscedastic** noise (σ^2 constant), the data term is proportional to the MSE up to an additive constant; in practice the fit-regularization trade-off can be tuned either by setting σ^2 or, equivalently, by adjusting β to re-balance the data term against the KL.

Since our main focus is on uncertainty-aware metrics rather than cross-output correlations, in the experiments we restrict attention to $d_y = 1$ and use the isotropic homoscedastic case, with a single constant variance σ^2 that we absorb into β .

Scalar homoscedastic β -ELBO. Consider the latent-weight model

$$\theta \sim p_0(\theta), \quad y | x, \theta \sim \mathcal{N}(f_\theta(x), \sigma^2),$$

with a variational family $q_\phi(\theta | x)$ (IC-/LP-FDN). For one datum (x_i, y_i) the standard ELBO is

$$\log p(y_i | x_i) \geq \underbrace{\mathbb{E}_{q_\phi}[\log p(y_i | x_i, \theta)]}_{\text{data term}} - \underbrace{KL(q_\phi(\theta | x_i) \| p_0(\theta))}_{\text{regularizer}}.$$

Using the Gaussian likelihood,

$$\log p(y_i | x_i, \theta) = -\frac{1}{2\sigma^2} (y_i - f_\theta(x_i))^2 - \frac{1}{2} \log(2\pi\sigma^2).$$

Plugging into the bound and negating yields the per-example loss

$$\mathcal{L}_{\text{ELBO}}^{(i)} = \frac{1}{2\sigma^2} \mathbb{E}_{q_\phi(\theta|x_i)}[(y_i - f_\theta(x_i))^2] + KL(q_\phi(\theta | x_i) \| p_0(\theta)) + \frac{1}{2} \log(2\pi\sigma^2).$$

Using K reparameterized samples $\theta^{(k)} \sim q_\phi(\theta | x_i)$ gives the unbiased Monte Carlo estimator

$$\mathcal{L}_{\text{ELBO}}^{(i)} \approx \frac{1}{2K\sigma^2} \sum_{k=1}^K (y_i - f_{\theta^{(k)}}(x_i))^2 + KL(q_\phi(\theta | x_i) \| p_0(\theta)) + \frac{1}{2} \log(2\pi\sigma^2).$$

Since $\frac{1}{2} \log(2\pi\sigma^2)$ does not depend on ϕ or θ , it can be dropped during optimization. If σ^2 is fixed, the data term is just a rescaled MSE, so

$$(2\sigma^2) \mathcal{L}_{\text{ELBO}}^{(i)} \doteq \frac{1}{K} \sum_{k=1}^K (y_i - f_{\theta^{(k)}}(x_i))^2 + \underbrace{(2\sigma^2)}_{\beta} KL(q_\phi(\theta | x_i) \| p_0(\theta)),$$

showing that choosing constant σ^2 is equivalent to training with a β -ELBO, with β simply rescaling the effective KL weight (capacity control). In this paper we directly use a β -ELBO for training.

Heteroscedastic observation model (scalar case). If we allow the observation variance to depend on x and the sampled weights θ ,

$$Y \mid x, \theta \sim \mathcal{N}(f_\theta(x), \sigma_\theta^2(x)) \quad (d_y = 1),$$

the per-example β -ELBO becomes

$$\mathcal{L}_{\text{het}}^{(i)} = \frac{1}{2K} \sum_{k=1}^K \left[\frac{(y_i - f_{\theta^{(k)}}(x_i))^2}{\sigma_{\theta^{(k)}}^2(x_i)} + \log(2\pi \sigma_{\theta^{(k)}}^2(x_i)) \right] + \beta KL(q_\phi(\theta \mid x_i) \parallel p_0(\theta)),$$

i.e., a weighted least-squares (WLS) term plus a variance penalty, with weights $w^{(k)}(x_i) = 1/\sigma_{\theta^{(k)}}^2(x_i)$ learned jointly with the mean.

Parameterization and stability. We parameterize

$$\sigma_\theta(x) = \varepsilon + \text{softplus}(\rho_\theta(x)), \quad \varepsilon = 10^{-3},$$

which guarantees positivity and avoids numerical collapse. To mitigate variance blow-up in early training, one can (i) apply gentle weight decay on ρ_θ , (ii) clip $s_\theta(x) = \log \sigma_\theta^2(x)$ to a reasonable range, or (iii) use a short β warm-up so the likelihood term dominates initially.

Predictive variance decomposition. Let $\theta \sim q_\phi(\theta \mid x)$ and, given (x, θ) ,

$$Y \mid x, \theta \sim \mathcal{N}(\mu_\theta(x), \sigma_\theta^2(x)).$$

Scalar case. The predictive (marginal) variance decomposes as

$$\text{Var}[Y \mid x] = \underbrace{\mathbb{E}_{\theta \sim q_\phi}[\sigma_\theta^2(x)]}_{\text{aleatoric}} + \underbrace{\text{Var}_{\theta \sim q_\phi}[\mu_\theta(x)]}_{\text{epistemic}}. \quad (6)$$

Proof. By the law of total expectation, $\mathbb{E}[Y \mid x] = \mathbb{E}_\theta[\mathbb{E}[Y \mid x, \theta]] = \mathbb{E}_\theta[\mu_\theta(x)]$. By the law of total variance,

$$\text{Var}[Y \mid x] = \mathbb{E}_\theta[\text{Var}(Y \mid x, \theta)] + \text{Var}_\theta(\mathbb{E}[Y \mid x, \theta]) = \mathbb{E}_\theta[\sigma_\theta^2(x)] + \text{Var}_\theta[\mu_\theta(x)]. \quad \square$$

Vector-output version. For $Y \in \mathbb{R}^{d_y}$ with $Y \mid x, \theta \sim \mathcal{N}(\mu_\theta(x), \Sigma_\theta(x))$ the predictive covariance is

$$\text{Cov}[Y \mid x] = \underbrace{\mathbb{E}_\theta[\Sigma_\theta(x)]}_{\text{aleatoric}} + \underbrace{\text{Cov}_\theta[\mu_\theta(x)]}_{\text{epistemic}}, \quad (7)$$

obtained by the matrix form of the law of total variance.

Monte Carlo estimators. With samples $\theta^{(k)} \sim q_\phi(\theta \mid x)$ we estimate the predictive mean and epistemic variance as

$$\hat{\mu}(x) = \frac{1}{K} \sum_{k=1}^K \mu_{\theta^{(k)}}(x), \quad \widehat{\text{Var}}_{\text{epi}}(x) = \frac{1}{K} \sum_{k=1}^K (\mu_{\theta^{(k)}}(x) - \hat{\mu}(x))^2,$$

and obtain the total predictive variance via the decomposition (6),

$$\widehat{\text{Var}}[Y \mid x] = \frac{1}{K} \sum_{k=1}^K \sigma_{\theta^{(k)}}^2(x) + \widehat{\text{Var}}_{\text{epi}}(x).$$

For $d_y > 1$, replace squared deviations by outer products to estimate covariances, in accordance with (7).

In our experiments we use the homoscedastic scalar case ($\sigma_\theta^2(x) \equiv \sigma^2$), so the aleatoric variance reduces to a constant and all input-dependent variability in $\text{Var}[Y \mid x]$ comes from the epistemic component $\text{Var}_\theta[\mu_\theta(x)]$; the heteroscedastic extension above is included for completeness.

E. FDN Training and Prediction Algorithm

Algorithm 1 FDN (Unified for IC-/LP-FDN): Training and Prediction

- 1: **Inputs:** dataset $\mathcal{D} = \{(x_i, y_i)\}_{i=1}^N$; base net f_θ with layers 1: L ; per-layer samplers $q_\phi^l(\theta_l | c_l)$ (diag. Gaussians); prior $p_0(\theta) = \prod_l p_0^l(\theta_l)$; MC K ; KL schedule $\{\beta_t\}$; variant $v \in \{\text{IC}, \text{LP}\}$.
 - 2: **for** step $t = 1, 2, \dots$ **do**
 - 3: Sample minibatch \mathcal{B} ; set $\Sigma_{\text{NLL}} \leftarrow 0, \Sigma_{\text{KL}} \leftarrow 0$
 - 4: **for** each $(x, y) \in \mathcal{B}$ **do**
 - 5: **for** $k = 1, \dots, K$ **do**
 - 6: $h_0^{(k)} \leftarrow x$
 - 7: **for** $l = 1, \dots, L$ **do**
 - 8: $c_l \leftarrow \begin{cases} x & \text{if } v = \text{IC} \\ h_{l-1}^{(k)} & \text{if } v = \text{LP} \end{cases}$
 - 9: $\varepsilon_l^{(k)} \sim \mathcal{N}(0, I), \quad \theta_l^{(k)} \leftarrow \mu_\phi^l(c_l) + \sigma_\phi^l(c_l) \odot \varepsilon_l^{(k)}$
 - 10: $h_l^{(k)} \leftarrow \text{layer}_l(h_{l-1}^{(k)}; \theta_l^{(k)})$
 - 11: $\Sigma_{\text{KL}} += KL(q_\phi^l(\theta_l | c_l) \| p_0^l(\theta_l))$
 - 12: **end for**
 - 13: $(\mu^{(k)}, \Sigma^{(k)}) \leftarrow \text{head}(h_L^{(k)})$ $\{\Sigma^{(k)}$ may be fixed (homoscedastic) $\}$
 - 14: $\ell_k \leftarrow \log \mathcal{N}(y; \mu^{(k)}, \Sigma^{(k)})$
 - 15: **end for**
 - 16: $\Sigma_{\text{NLL}} += -\frac{1}{K} \sum_{k=1}^K \ell_k$ $\{\text{ELBO (mean-of-logs)}\}$
 - 17: **end for**
 - 18: $\mathcal{L} \leftarrow \frac{1}{N} (\Sigma_{\text{NLL}} + \beta_t \Sigma_{\text{KL}})$; update ϕ by backprop on \mathcal{L}
 - 19: **end for**
 - 20: **Predict at** x_\star : repeat the per-layer sampling with $c_l = \{x_\star \text{ or } h_{l-1}^{(k)}\}$ per v to obtain $(\mu_\star^{(k)}, \Sigma_\star^{(k)})$, and return $\hat{p}(y | x_\star) \approx \frac{1}{K} \sum_k \mathcal{N}(y; \mu_\star^{(k)}, \Sigma_\star^{(k)})$.
-

F. Supplementary Figures and Tables

In this appendix we provide additional qualitative diagnostics. Figure 6 and Figure 7 plot predictive means versus input for the toy and real tasks, respectively. Figure 8 and Figure 9 show aggregated MSE–variance scatter plots complementing Figure 2 and Figure 3 in the main text, while Figure 10 and Figure 11 report full risk–coverage curves (AURC) for toy and real datasets, complementing the summary statistics in Table 5, Table 6, Table 7, Table 8, Table 9, and Table 10.

Table 2. Monte Carlo and training Hyperparameters (defaults unless noted).

Component	Symbol	Setting
MC samples (train)	K_{train}	1
MC samples (validate)	K_{val}	100
MC samples (test)	K_{test}	100
Epochs	ϵ	400
Optimizer	—	ADAM
Learning rate	η	1×10^{-3}
Batch size	B	64
Weight prior std	σ_0	1.0
Variance floor	ε	10^{-3} in $\sigma = \varepsilon + \text{softplus}(\rho)$
KL schedule	β_t	linear
Maximum β	β_{max}	1.0
Warm up updates	—	200
Toy Grid Seed	—	0
Step Seed	—	13
Sine Seed	—	19
Quadratic Seed	—	6
Airfoil Self-Noise Seed	—	64
CCPP Power Plant Seed	—	2
Energy Efficiency Heating Seed	—	2
Stochastic Checkpoint	—	minimum CRPS in interpolation
Deterministic Checkpoint	—	minimum MSE in interpolation

Table 3. Number of training, validation, and test examples used for the toy 1D regression tasks and the three UCI real datasets.

Dataset	N_{train}	N_{val}	N_{test}	N_{total}
Toy 1D functions	1024	512	2001	3537
Airfoil Self-Noise	597	199	707	1503
CCPP Power Plant	3444	1148	4976	9568
Energy Efficiency (heating load)	307	102	359	768

Table 4. Model configurations and compute. Columns: base hidden width d_{hid} ; hypernetwork hidden width d_{hyper} ; latent dim d_h (for Gaussian Hypernetwork); ensemble size M ; parameter count P (per model). Use “—” where not applicable.

Model	d_{hid}	d_{hyper}	d_h	M	P
MLPDropoutNet	333	—	—	1	1000
Deep Ensemble	64	—	—	10	1000
BayesNet	166	—	—	1	998
Gaussian HyperNet	24	5	9	1	994
IC-FDNet	23	6	—	1	1004
LP-FDNet	24	5	—	1	1011

Notes. We can see that the parameter count is roughly equal. In order to keep a fair comparison we scale the number of epochs by the ensemble size so the number of updates is roughly the same.

Functional Distribution Networks (FDN)

Table 5. Step function: unified calibration/uncertainty summary. Lower is better for AURC and deltas ($\Delta=$ OOD-ID); ideal MSE-Var fit has $a \approx 0, b \approx 1$.

Model	ρ	b	a	AURC \downarrow	Δ Var (OOD-ID) \uparrow	Δ MSE (OOD-ID) \downarrow	Δ CRPS (OOD-ID) \downarrow
MLPDropoutNet	0.990	1.34	-0.02	1.1	2.7	3.6	0.433
DeepEnsembleNet	0.986	4.39	-0.08	3.1	2.6	11.3	1.579
BayesNet	0.987	71.82	-3.50	8.2	0.4	29.6	4.081
GaussHyperNet	1.000	1.02	0.59	54.0	167.3	169.8	2.386
IC-FDNet	0.992	2.52	-475.80	373.1	1725.4	3820.5	16.230
LP-FDNet	1.000	1.04	-17.93	468.5	6306.7	6529.4	8.774

Table 6. Sine function: unified calibration/uncertainty summary. Lower is better for AURC and deltas ($\Delta=$ OOD-ID); ideal MSE-Var fit has $a \approx 0, b \approx 1$.

Model	ρ	b	a	AURC \downarrow	Δ Var (OOD-ID) \uparrow	Δ MSE (OOD-ID) \downarrow	Δ CRPS (OOD-ID) \downarrow
MLPDropoutNet	0.966	32.68	476.11	1178.4	112.6	4209.7	50.061
DeepEnsembleNet	0.632	1.16	1.16	1.5	1.0	1.1	-0.179
BayesNet	0.999	1.00	1.20	19.7	55.7	55.7	1.066
GaussHyperNet	1.000	1.02	0.85	59.0	183.8	187.0	2.265
IC-FDNet	0.973	1.73	1098.34	623.4	1436.3	3705.1	20.842
LP-FDNet	0.999	1.05	38.14	382.9	3170.0	3362.4	6.527

Table 7. Quadratic function: unified calibration/uncertainty summary. Lower is better for AURC and deltas ($\Delta=$ OOD-ID); ideal MSE-Var fit has $a \approx 0, b \approx 1$.

Model	ρ	b	a	AURC \downarrow	Δ Var (OOD-ID) \uparrow	Δ MSE (OOD-ID) \downarrow	Δ CRPS (OOD-ID) \downarrow
MLPDropoutNet	0.990	3459.12	-67.32	38.7	0.1	231.7	11.176
DeepEnsembleNet	0.979	811.63	-68.32	56.4	0.5	306.2	13.003
BayesNet	0.953	3855.46	-89.49	81.3	0.1	389.1	15.136
GaussHyperNet	0.993	2.81	-112.41	142.5	253.9	603.6	9.137
IC-FDNet	0.988	1.42	225.67	377.8	1743.9	2721.7	14.073
LP-FDNet	0.997	1.42	-107.08	308.6	2547.3	3510.6	10.325

Table 8. Airfoil Self-Noise: unified calibration/uncertainty summary. Lower is better for AURC and deltas ($\Delta=$ OOD-ID); ideal MSE-Var fit has $a \approx 0, b \approx 1$.

Model	ρ	b	a	AURC \downarrow	Δ Var (OOD-ID) \uparrow	Δ MSE (OOD-ID) \downarrow	Δ CRPS (OOD-ID) \downarrow
MLPDropoutNet	0.601	10.14	0.21	0.4	0.1	1.1	0.535
DeepEnsembleNet	0.177	9.74	0.57	0.6	0.0	0.8	0.353
BayesNet	0.330	4.49	0.40	0.7	0.2	1.1	0.335
GaussHyperNet	0.987	1.01	0.90	10.0	18.9	19.1	0.340
IC-FDNet	0.976	1.40	-3.40	7.6	19.4	25.3	0.493
LP-FDNet	0.983	1.00	1.01	9.3	28.5	28.8	0.363

Table 9. CCPP Power Plant: unified calibration/uncertainty summary. Lower is better for AURC and deltas ($\Delta=$ OOD-ID); ideal MSE-Var fit has $a \approx 0, b \approx 1$.

Model	ρ	b	a	AURC \downarrow	Δ Var (OOD-ID) \uparrow	Δ MSE (OOD-ID) \downarrow	Δ CRPS (OOD-ID) \downarrow
MLPDropoutNet	0.417	6.07	0.083	0.142	0.023	0.156	0.095
DeepEnsembleNet	0.126	20.05	0.127	0.139	0.002	0.071	0.065
BayesNet	0.470	1.75	0.099	0.201	0.065	0.132	0.045
GaussHyperNet	0.998	1.02	0.108	4.884	7.134	7.159	0.283
IC-FDNet	0.970	1.20	-0.303	2.731	2.916	3.401	0.211
LP-FDNet	0.902	0.99	0.903	2.844	2.129	2.820	0.260

Table 10. Energy Efficiency: unified calibration/uncertainty summary. Lower is better for AURC and deltas ($\Delta=$ OOD-ID); ideal MSE-Var fit has $a \approx 0, b \approx 1$.

Model	ρ	b	a	AURC \downarrow	Δ Var (OOD-ID) \uparrow	Δ MSE (OOD-ID) \downarrow	Δ CRPS (OOD-ID) \downarrow
MLPDropoutNet	0.696	4.42	0.00	0.1	0.0	0.3	0.258
DeepEnsembleNet	0.426	7.58	0.01	0.1	0.0	0.0	0.051
BayesNet	0.549	4.13	-0.10	0.2	0.0	0.1	0.106
GaussHyperNet	0.996	1.04	0.42	32.4	30.3	30.9	0.454
IC-FDNet	0.993	1.02	0.26	14.1	6.6	6.8	0.114
LP-FDNet	0.989	0.97	1.45	14.1	6.8	6.2	0.005

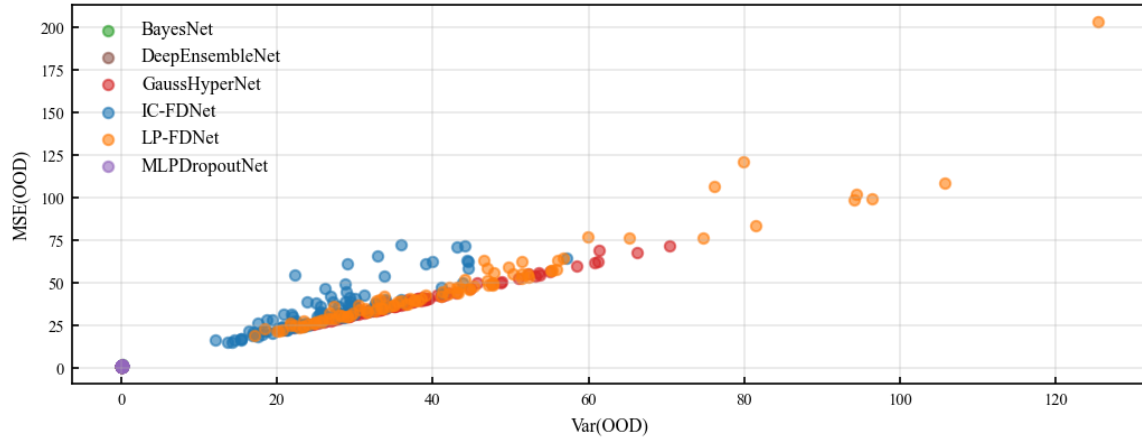
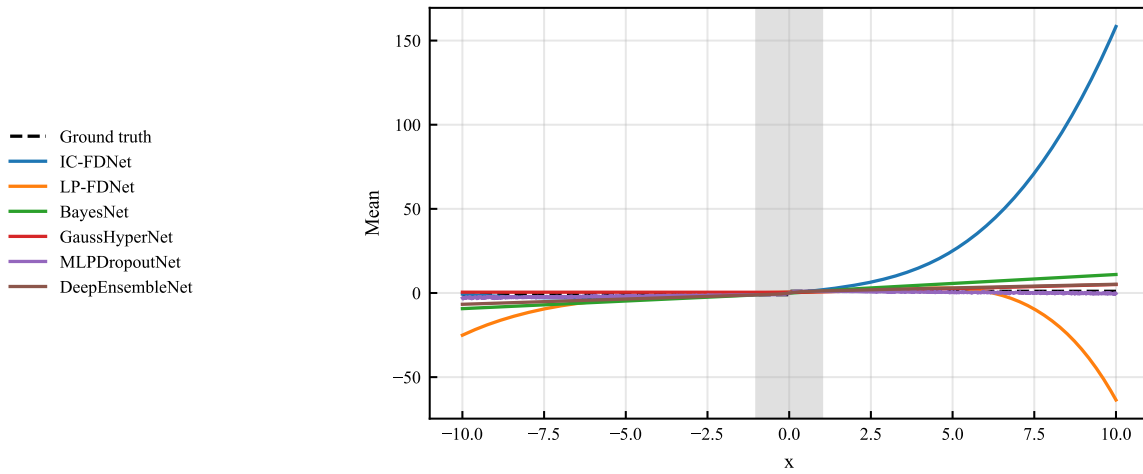
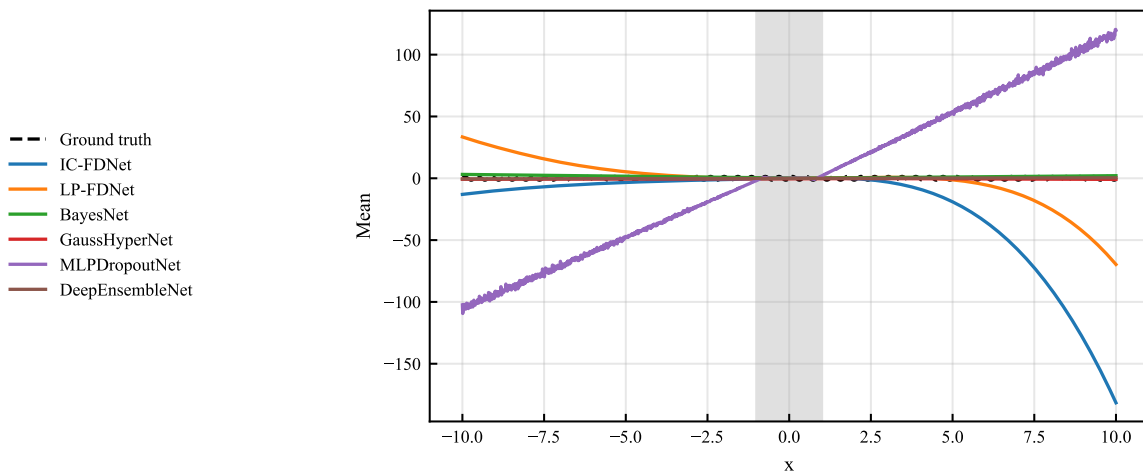


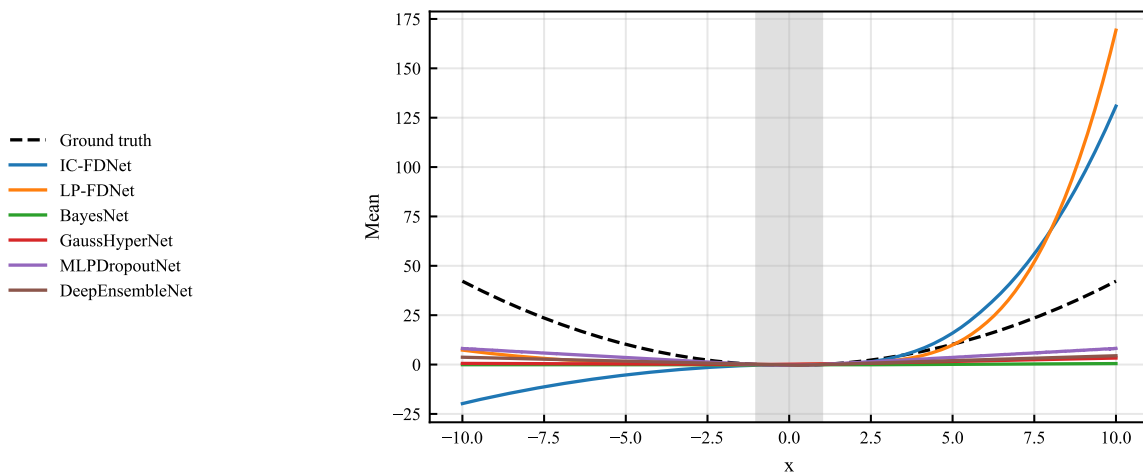
Figure 5. Seed-aggregated MSE–variance scatter on the Airfoil Self-Noise dataset over 100 random initializations. Each point summarizes one seed by its OOD MSE and OOD predictive variance, and the representative seed used in the main-text plots lies close to the overall across-seed trend.



(a) Step: $H(x)$

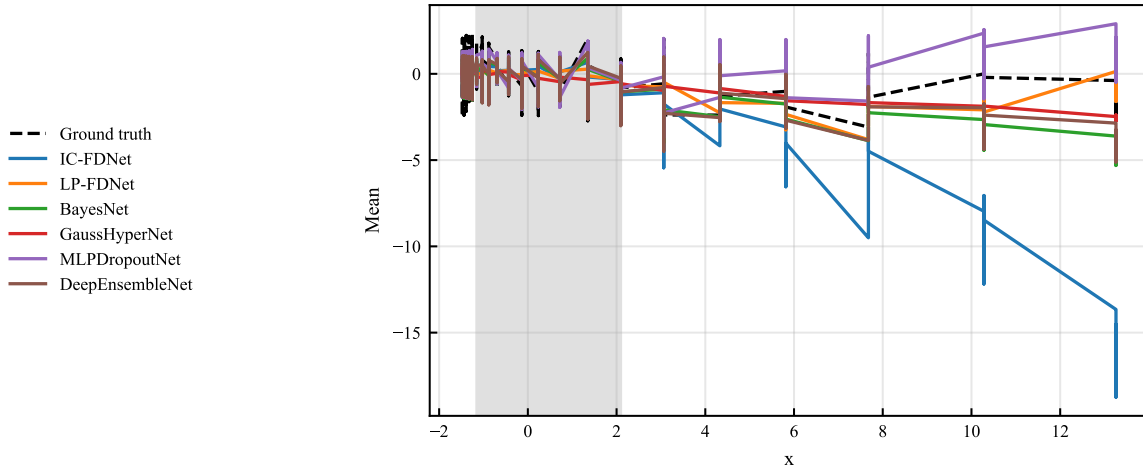


(b) Sine: $1.54 \sin(2.39 x)$

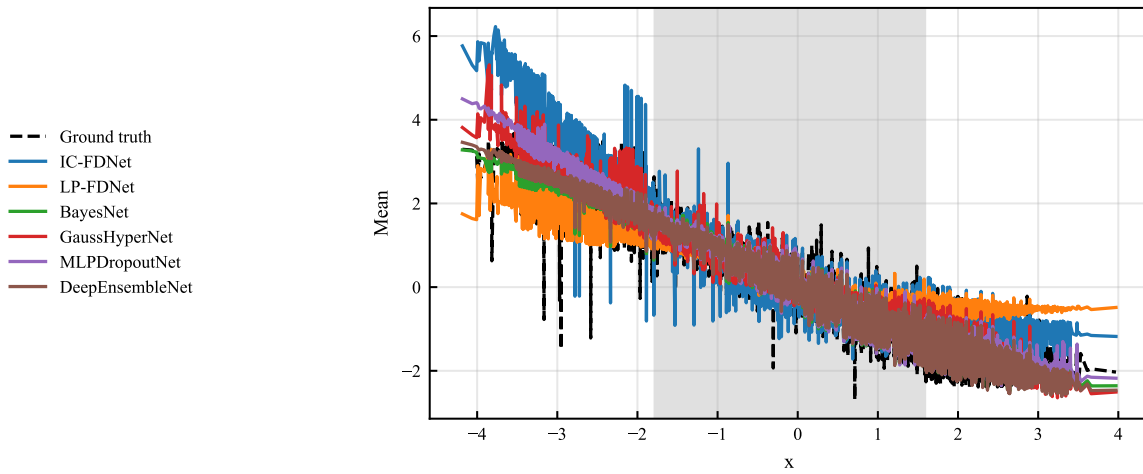


(c) Quadratic: $0.43x^2 - 0.41$

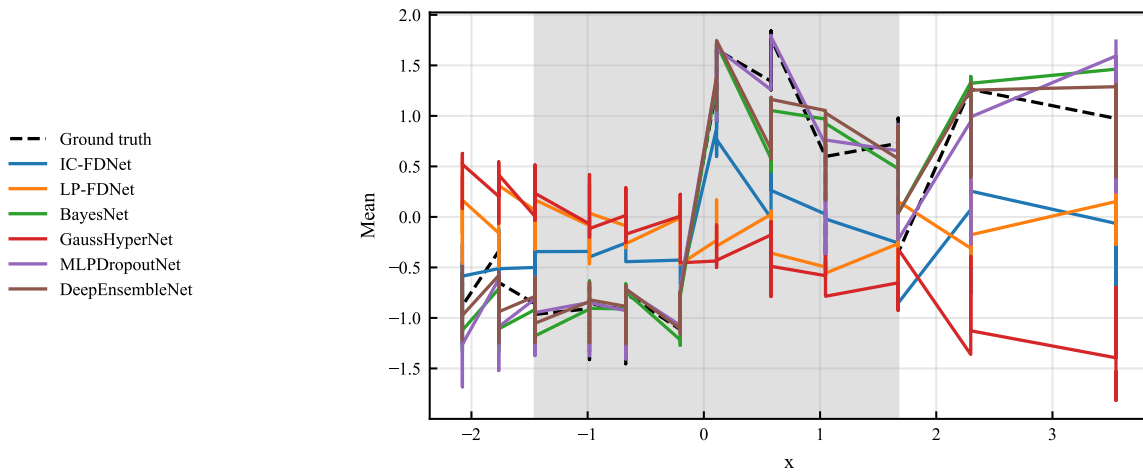
Figure 6. Predictive mean vs. input x for the three synthetic 1D toy tasks (step, sine, quadratic), with the ground-truth function overlaid. Shaded region corresponds to the interpolation/ ID points.



(a) Airfoil Self-Noise



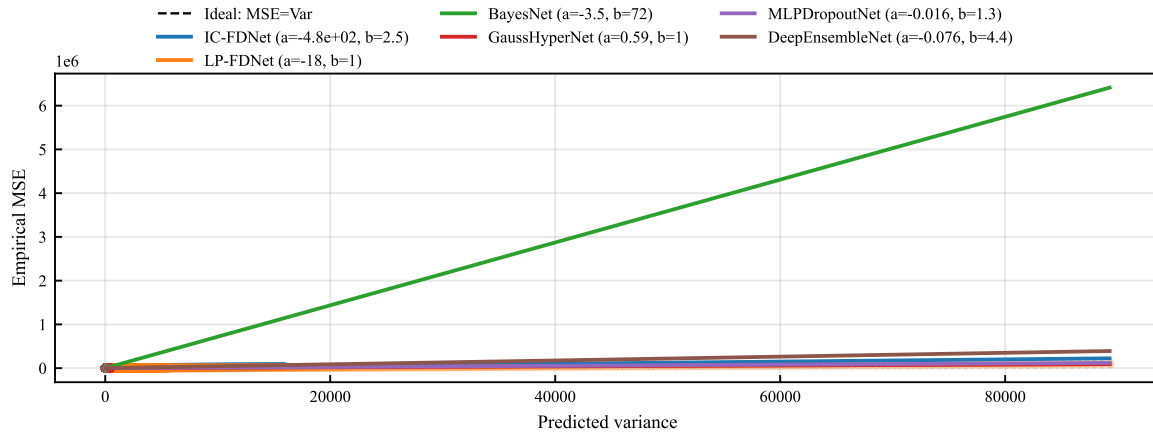
(b) CCPP Power Plant



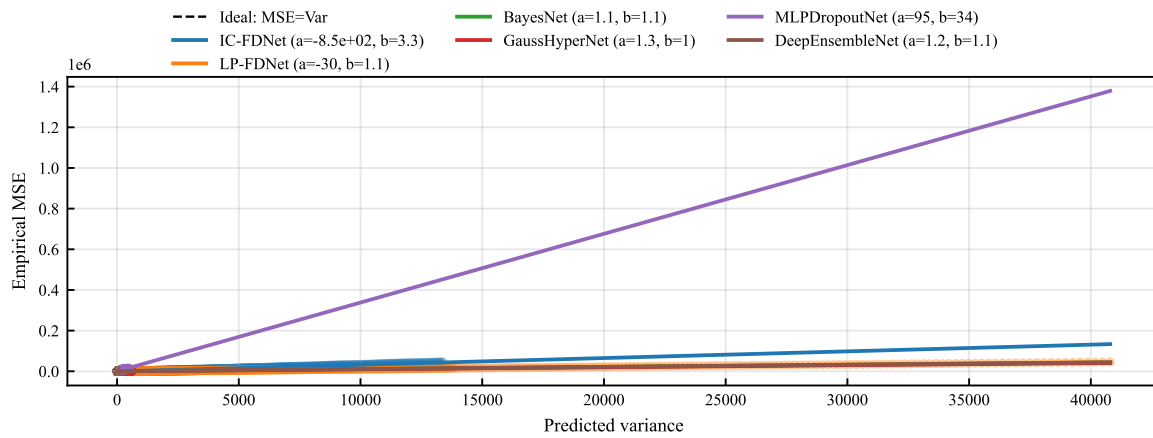
(c) Energy Efficiency

Figure 7. Predictive mean vs. standardized split feature x for the three real regression datasets (Airfoil Self-Noise, CCPP Power Plant, Energy Efficiency). Shaded region corresponds to the interpolation/ ID points.

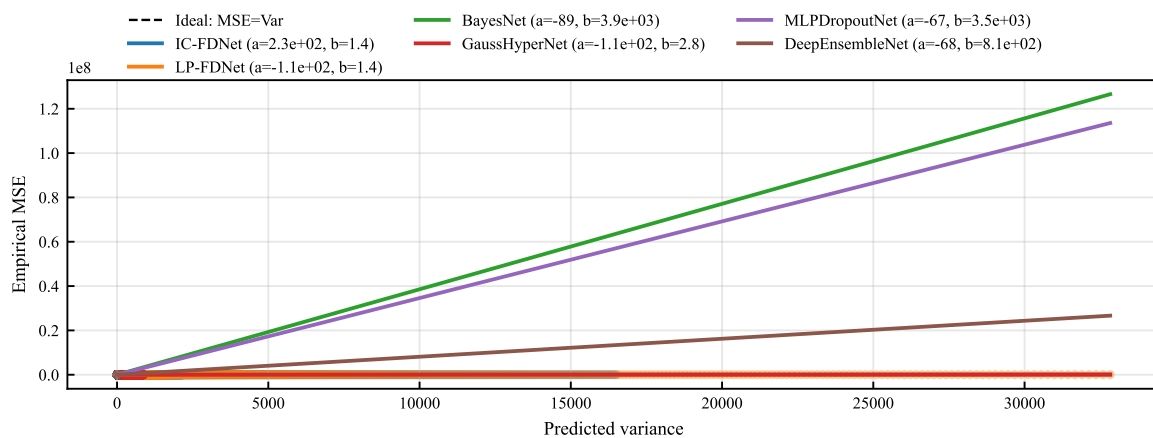
Functional Distribution Networks (FDN)



(a) Step: $H(x)$

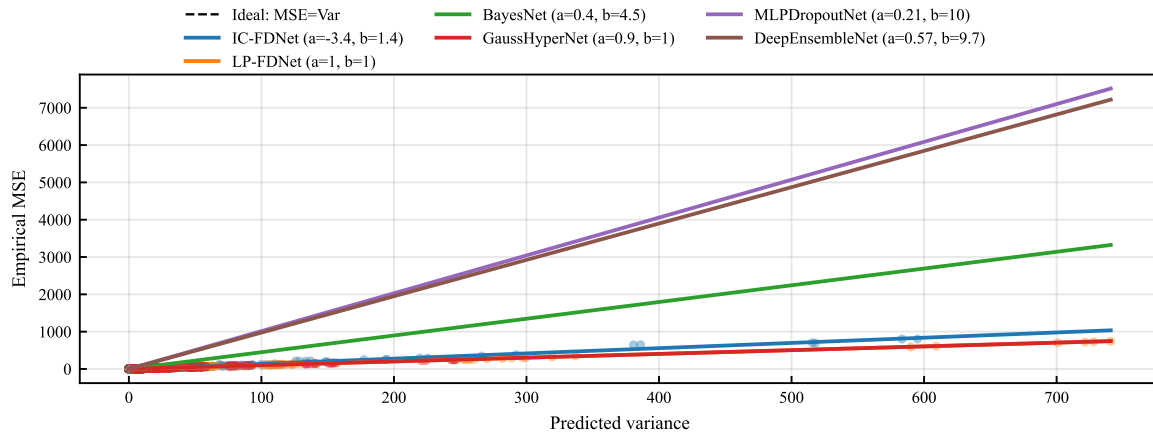


(b) Sine: $1.54 \sin(2.39x)$

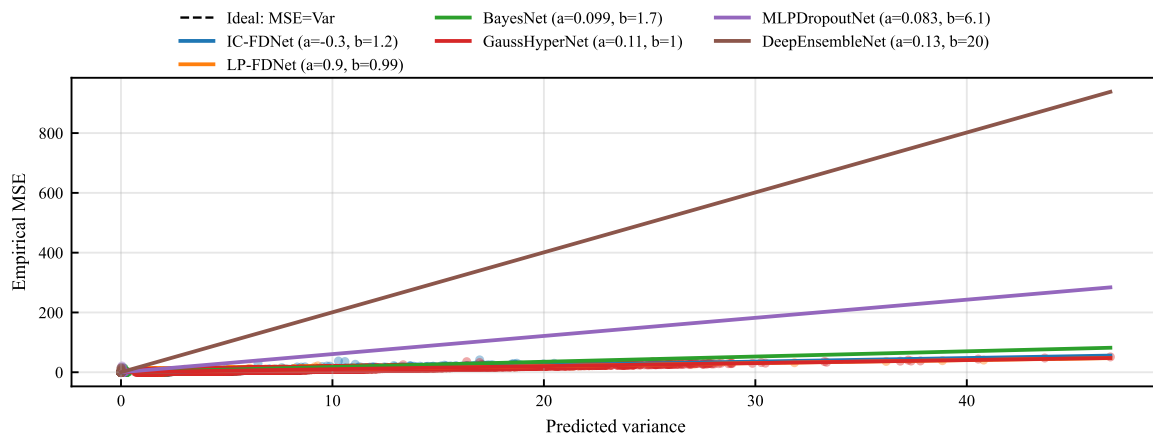


(c) Quadratic: $0.43x^2 - 0.41$

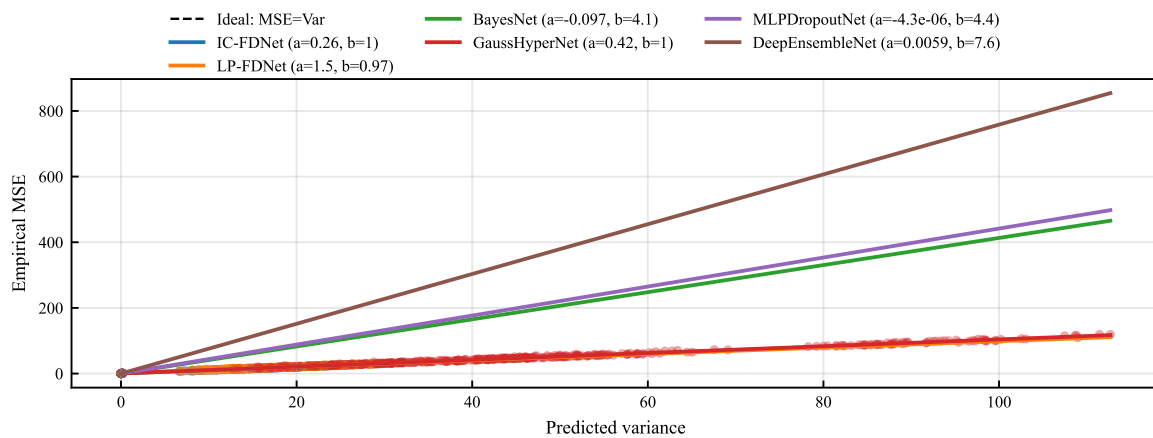
Figure 8. MSE vs. predicted variance scatter plots for the three toy tasks. Each panel aggregates ID and OOD test points; the dashed line shows the ideal calibration $MSE = Var$. Legends in the PDFs report Spearman's ρ and linear-fit slope/intercept.



(a) Airfoil Self-Noise



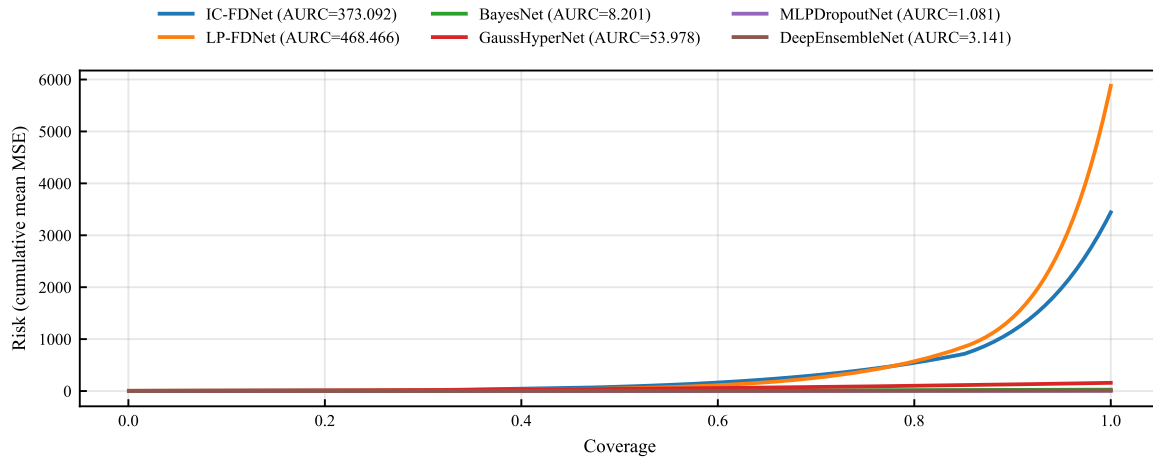
(b) CCGP Power Plant



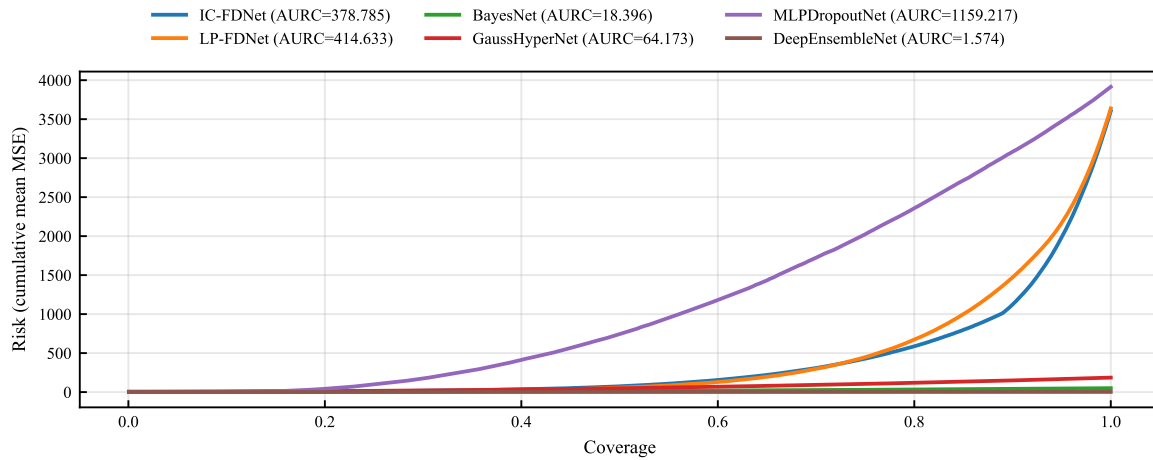
(c) Energy Efficiency

Figure 9. MSE vs. predicted variance scatter plots for the three real datasets. The dashed line marks $MSE = Var$; legends report Spearman's ρ and linear-fit parameters.

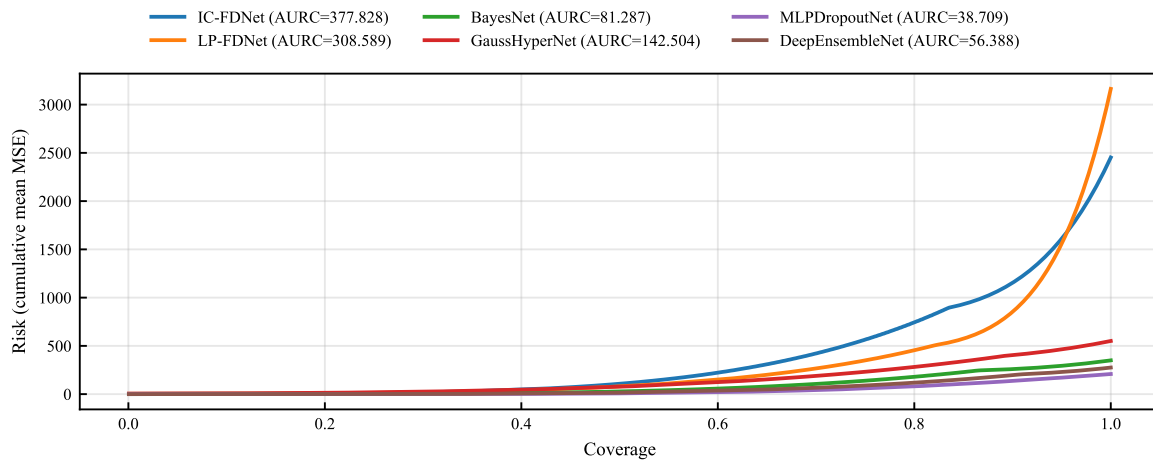
Functional Distribution Networks (FDN)



(a) Step: $H(x)$

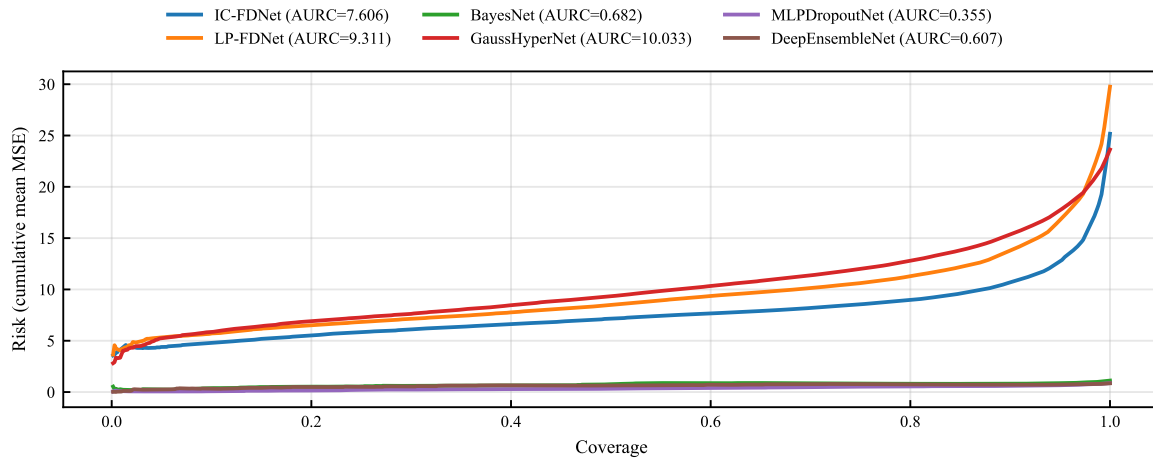


(b) Sine: $1.54 \sin(2.39 x)$

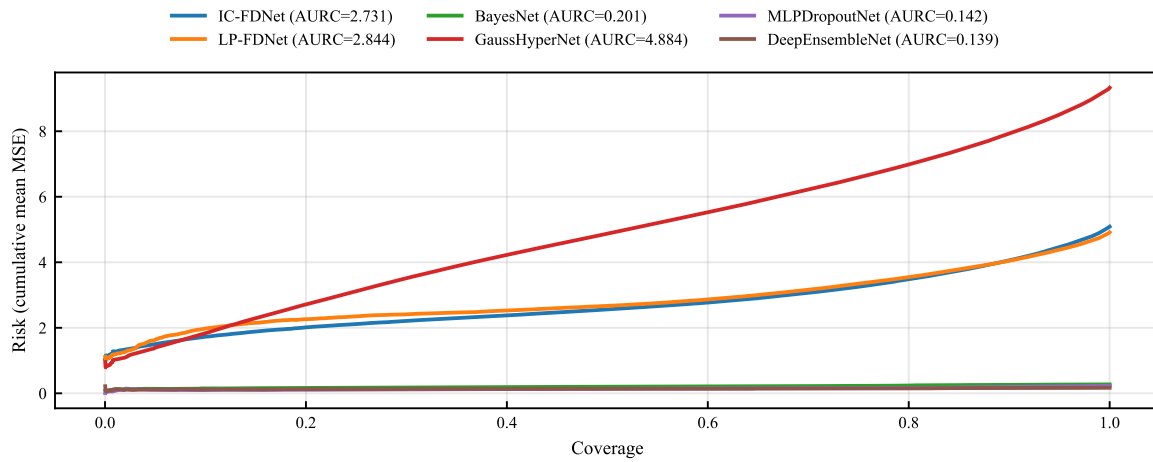


(c) Quadratic: $0.43x^2 - 0.41$

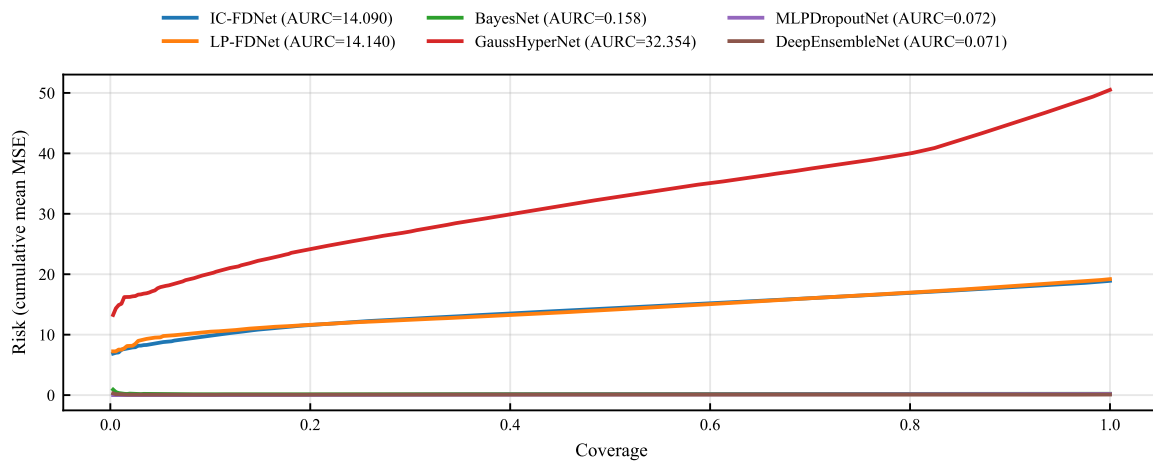
Figure 10. Risk–coverage curves (AURC) for the three toy tasks. Curves plot average squared error as a function of coverage as high-variance predictions are rejected. Lower AURC indicates better selective regression.



(a) Airfoil Self-Noise



(b) CCGP Power Plant



(c) Energy Efficiency

Figure 11. Risk–coverage curves (AURC) for the three real datasets. Lower area under the curve indicates better ability to abstain on high-error points as coverage decreases.

G. Computational complexity and scalability

Deterministic MLP. Let N denote the number of training examples, d_x the input dimension, d_y the output dimension, and consider a base network with widths $\{d_\ell\}_{\ell=0}^L$ with $d_0 = d_x, d_L = d_y$. A deterministic MLP has per-epoch cost

$$O\left(N \sum_{\ell=1}^L d_{\ell-1} d_\ell\right),$$

i.e., linear in N and quadratic in the layer widths.

FDN and Hypernetworks. FDN replaces each fixed weight matrix by an input-conditioned diagonal Gaussian $q_\phi(W_\ell, b_\ell | s_\ell(x))$ whose parameters are generated by a small per-layer Hypernetwork. For layer ℓ , the Hypernetwork takes a conditioning vector

$$s_\ell(x) = \begin{cases} x, & \text{IC-FDN,} \\ a_{\ell-1}(x), & \text{LP-FDN,} \end{cases}$$

with dimension $d_{s,\ell} \in \{d_x, d_{\ell-1}\}$, and outputs $(\mu_{W_\ell}, \log \sigma_{W_\ell}^2, \mu_{b_\ell}, \log \sigma_{b_\ell}^2) \in \mathbb{R}^{P_\ell}$, where $P_\ell = 2(d_{\ell-1}d_\ell + d_\ell)$. In our implementation, each Hypernetwork A_ℓ is a two-layer MLP with hidden width h_{hyp} . For a mini-batch of size B and K Monte Carlo samples per example, the per-epoch complexity is

$$O\left(NK \sum_{\ell=1}^L (d_{s,\ell} h_{\text{hyp}} + h_{\text{hyp}} P_\ell + d_{\ell-1} d_\ell)\right).$$

The three bracketed terms correspond to (i) the Hypernetwork input transform, (ii) projection to the P_ℓ Gaussian parameters, and (iii) the base-layer matrix–vector product. In all experiments we use $K = 1$ and small Hypernetwork widths (chosen to satisfy a global $\approx 10^3$ parameter budget), making $h_{\text{hyp}} P_\ell$ comparable to $d_{\ell-1} d_\ell$. As a result: (i) the training cost of IC-/LP-FDN remains linear in N ; (ii) the runtime overhead relative to a deterministic MLP is a small constant factor (typically 2–4 \times), set by h_{hyp} and K .

Parameter-count clarification. A concern raised in the reviews was that LP-FDN parameter count might scale cubically in model size (e.g., as $O(d_\ell^3)$ in the width of a layer). This would occur only for a specific design where the Hypernetwork directly maps a d_ℓ -dimensional activation to all d_ℓ^2 entries of a dense weight matrix via a fully connected layer, which would require a $d_\ell^2 \times d_\ell$ matrix.

In our implementation, however, the Hypernetwork hidden width h_{hyp} is a small constant, independent of d_ℓ :

$$P_\ell^{\text{hyper}} = d_{s,\ell} h_{\text{hyp}} + h_{\text{hyp}} \cdot 2(d_{\ell-1} d_\ell + d_\ell) \sim O(h_{\text{hyp}} d_{\ell-1} d_\ell) \sim O(d_{\ell-1} d_\ell).$$

Thus IC-FDN and LP-FDN both have the same $O(d_{\ell-1} d_\ell)$ scaling as the corresponding base MLP layer; in particular, there is no cubic dependence on layer width.

Architectural trade-offs for larger scales. FDN is compatible with standard complexity-reduction techniques without changing the formulation: (i) low-rank factorizations $W_\ell = U_\ell V_\ell^\top$ with the Hypernetwork generating only (U_ℓ, V_ℓ) ; (ii) row- or column-wise generation instead of full matrices; and (iii) a shared Hypernetwork with layer-specific output heads. In the main experiments we keep the architecture minimal to match parameter and update budgets across baselines, but these options make FDN readily extendable to higher-dimensional and large- N settings.

Middle-layer usage and adapter-style deployment. In practice, Hypernetworks need not be applied to *every* layer of a deep backbone. FDN is layer-local, so one can restrict stochastic, input-conditioned weights to a small subset of higher layers (or even just the predictive head), keeping earlier blocks deterministic and frozen. This is analogous in spirit to LoRA and adapter modules (Hu et al., 2022; Houlsby et al., 2019): a narrow, trainable “uncertainty adapter” is inserted on top of a largely fixed backbone, so the additional parameters and compute scale with the adapter width rather than with the full network depth or width. In such configurations the overall parameter and FLOP overhead of FDN remains a small fraction of the backbone, even for large architectures, while still enabling input-dependent uncertainty where it is most needed.

H. Evaluation metrics and calibration diagnostics

For a test set $\{(x_i, y_i)\}_{i=1}^T$ and a stochastic predictor that yields K samples $\{y_i^{(k)}\}_{k=1}^K$ from the predictive distribution $p(y | x_i, \mathcal{D})$, we use the following metrics.

Point prediction error. The predictive mean at x_i is

$$\hat{\mu}_i = \frac{1}{K} \sum_{k=1}^K y_i^{(k)}.$$

We define the *per-point* Monte Carlo MSE and bias as

$$\text{MSE}_i = \frac{1}{K} \sum_{k=1}^K (y_i^{(k)} - y_i)^2, \quad \text{Bias}_i = \hat{\mu}_i - y_i = \frac{1}{K} \sum_{k=1}^K (y_i^{(k)} - y_i).$$

For any subset of test inputs $S \subseteq \{1, \dots, T\}$ (e.g., all, ID, or OOD), we aggregate by averaging over $i \in S$:

$$\text{MSE}_S = \frac{1}{|S|} \sum_{i \in S} \text{MSE}_i, \quad \text{Bias}_S = \frac{1}{|S|} \sum_{i \in S} \text{Bias}_i.$$

Unless otherwise noted, reported MSE and Bias refer to these region-averaged quantities.

Predictive variance and epistemic uncertainty. The Monte Carlo estimator of predictive variance at x_i is

$$\widehat{\text{Var}}[Y | x_i] = \frac{1}{K} \sum_{k=1}^K (y_i^{(k)} - \hat{\mu}_i)^2,$$

which we aggregate over ID or OOD test splits by averaging across i . In the homoscedastic Gaussian setting this decomposes into aleatoric and epistemic components via the law of total variance; we focus on the epistemic part induced by the weight distribution.

Continuous ranked probability score (CRPS). For a univariate predictive CDF $F_i(y)$ and realization y_i , the CRPS is

$$\text{CRPS}(F_i, y_i) = \int_{-\infty}^{\infty} (F_i(z) - \mathbf{1}\{z \geq y_i\})^2 dz.$$

Using samples $y_i^{(k)} \sim F_i$, we apply the standard Monte Carlo estimator

$$\widehat{\text{CRPS}}_i = \frac{1}{K} \sum_{k=1}^K |y_i^{(k)} - y_i| - \frac{1}{2K^2} \sum_{k=1}^K \sum_{\ell=1}^K |y_i^{(k)} - y_i^{(\ell)}|.$$

We report the average CRPS over ID and OOD test splits. Lower CRPS within a region (ID or OOD) indicates a sharper and better calibrated predictive distribution: mass is concentrated near y_i without being spuriously overconfident. Under shift we typically expect $\text{CRPS}_{\text{OOD}} > \text{CRPS}_{\text{ID}}$ because the task is harder; for a fixed OOD difficulty, smaller CRPS_{OOD} (or smaller ΔCRPS , see below) is better.

Calibration: MSE–variance relation. To assess calibration we compare the predicted variance $\widehat{\text{Var}}[Y | x_i]$ with the empirical per-point MSE

$$e_i = \text{MSE}_i = \frac{1}{K} \sum_{k=1}^K (y_i^{(k)} - y_i)^2.$$

We first compute Spearman rank correlation $\rho = \text{corr}_{\text{Spearman}}(\{\widehat{\text{Var}}_i\}, \{e_i\})$ and fit the linear relation $e_i \approx a + b \widehat{\text{Var}}_i$ by least squares; the ideal fit has $a \approx 0$ and $b \approx 1$. High ρ means that larger predicted variance reliably flags larger squared error (good ranking), while (a, b) measure the *scale* of the variances relative to the errors.

In addition, we form *variance–MSE calibration curves* by binning test points into B quantiles of predicted variance. In each bin b (with index set S_b) we compute the mean predicted variance $\text{Var}_b = \frac{1}{|S_b|} \sum_{i \in S_b} \widehat{\text{Var}}_i$ and empirical MSE $\text{MSE}_b = \frac{1}{|S_b|} \sum_{i \in S_b} \text{MSE}_i$, and plot the pairs $(\text{Var}_b, \text{MSE}_b)$ together with the ideal $y=x$ line. Points lying close to this diagonal indicate that the typical error magnitude in each confidence bin matches the predicted variance scale.

Risk–coverage (AURC). Using variance as an inverse-confidence score, we sort test points by increasing $\widehat{\text{Var}}[Y | x_i]$. For a coverage level $c \in (0, 1]$ (fraction of most-confident points retained) we compute the cumulative risk $R(c)$ as the average per-point MSE over the retained subset:

$$R(c) = \frac{1}{|S(c)|} \sum_{i \in S(c)} \text{MSE}_i,$$

where $S(c)$ contains the most-confident fraction c of test points. The area under the risk–coverage curve, $\text{AURC} = \int_0^1 R(c) dc$, is estimated numerically. Lower AURC is better: for a fixed difficulty, it means that as we keep only high-confidence predictions, the resulting risk drops more quickly.

ID vs. OOD deltas. For each model and dataset we compute MSE, variance, and CRPS separately on ID (interpolation) and OOD (extrapolation) regions, using the region averages defined above, and report

$$\Delta\text{MSE} = \text{MSE}_{\text{OOD}} - \text{MSE}_{\text{ID}}, \quad \Delta\text{Var} = \text{Var}_{\text{OOD}} - \text{Var}_{\text{ID}}, \quad \Delta\text{CRPS} = \text{CRPS}_{\text{OOD}} - \text{CRPS}_{\text{ID}}.$$

For a fixed notion of shift, good uncertainty estimates should exhibit small ΔMSE (robust accuracy), *large and positive* ΔVar (higher uncertainty OOD than ID), and small ΔCRPS (predictive distributions that degrade gracefully rather than collapsing or becoming wildly miscalibrated).

On NLL / NLPD. Negative log predictive density (NLL / NLPD) is another strictly proper scoring rule for probabilistic regression and is closely related to CRPS. We computed NLL in preliminary experiments, but found that in our setting it was (i) strongly correlated with CRPS and MSE, and (ii) much more sensitive to occasional extreme errors due to the logarithm, which can dominate the average and obscure more typical behavior. CRPS, by contrast, remains finite, can be estimated directly from samples without specifying a parametric density or bandwidth, and provides a more interpretable summary of the overall predictive distribution (both sharpness and calibration) under dataset shift. For these reasons, and to avoid redundant plots/tables, we report CRPS (together with MSE, variance, and AURC) as our primary proper scoring rule and omit NLL/NLPD from the main results.